



HAL
open science

Heavy halogen impact on Raman water bands at high pressure: Implications for salinity estimations in fluid inclusions

Tobias Grützner, Hélène Bureau

► **To cite this version:**

Tobias Grützner, Hélène Bureau. Heavy halogen impact on Raman water bands at high pressure: Implications for salinity estimations in fluid inclusions. *Chemical Geology*, 2024, 654, pp.122065. 10.1016/j.chemgeo.2024.122065 . hal-04560527

HAL Id: hal-04560527

<https://hal.science/hal-04560527>

Submitted on 26 Apr 2024

HAL is a multi-disciplinary open access archive for the deposit and dissemination of scientific research documents, whether they are published or not. The documents may come from teaching and research institutions in France or abroad, or from public or private research centers.

L'archive ouverte pluridisciplinaire **HAL**, est destinée au dépôt et à la diffusion de documents scientifiques de niveau recherche, publiés ou non, émanant des établissements d'enseignement et de recherche français ou étrangers, des laboratoires publics ou privés.

1 Heavy halogen impact on Raman water bands at high pressure:
2 implications for salinity estimations in fluid inclusions

3 Tobias Grützner^{1,2,3*}, Hélène Bureau¹

4

5 ¹ Institut de Minéralogie, de Physique des Matériaux et de Cosmochimie (IMPMC), Sorbonne
6 Université Paris, France.

7 ² Research School of Earth Sciences, Australian National University, Canberra, Australia.

8 ³ Institut für Geowissenschaften, Goethe-Universität Frankfurt, Germany.

9

10 *Corresponding author

11

12 Email addresses: tobias.gruetzner@outlook.com (T. Grützner), helene.bureau@sorbonne-
13 universite.fr (H. Bureau).

14

15

16 Abstract

17 We present a new experimental dataset on the impact of the heavy halogens chlorine, bromine
18 and iodine on the Raman water bands concerning pressure and their concentration at room
19 temperature. These experiments were conducted at ambient temperature, with variations in
20 halogen concentration and pressure ranging from 0 to 1.4 GPa.

21 The strength of the Raman water band shift change increases with the ionic size from chlorine,
22 over bromine, to iodine. Our experiments further demonstrate that increased pressure
23 diminishes the impact of the halogen shift change to a varying extent for each of the three
24 halogens. This finding can have significant implications for the salinity calculation of fluid
25 inclusions in minerals such as quartz or olivine. Particularly in the low salinity range, the
26 concentration can be markedly underestimated if the pressure effect is neglected. For
27 experiments in diamond anvil cells involving halogens dissolved in water, the change in Raman
28 water band shifts can serve either as a new tool to monitor pressure, or to monitor the salinity.

29

30

31 Keywords

32 Raman, water bands, Fluid inclusion, halogens, salinity, high pressure

33

34 1. Introduction

35 Halogens play a pivotal role as volatile elements, significantly impacting geodynamic
36 processes. They constitute essential components of volcanic fumaroles and volcanic ejecta.
37 Upon release into the atmosphere, halogens contribute to ozone destruction. In crustal
38 hydrothermal fluids, halogen complexes (e.g., in saline fluids, brines, or molten salts) serve as
39 major agents for metal transport in ore-forming processes related to hydrothermal systems
40 (e.g., Aiuppa et al., 2009). Samples of such fluids can be found entrapped as inclusions in
41 minerals like quartz (e.g., Brooks et al., 2019; Pankrushina et al., 2020) or olivine (e.g.,
42 Kawamoto et al., 2013) in magmatic and metamorphic rocks. Raman spectroscopy has been
43 employed for decades to determine the salinity of fluid inclusions, especially those too small
44 for other common techniques like microthermometry – a method that determines salinity by
45 observing and measuring the freezing temperature of the fluid (cf. e.g., Kawamoto et al., 2013;
46 Moncada and Bodnar, 2012; Brooks et al., 2019).

47 The Raman spectra of water and aqueous fluids exhibit several peaks closely grouped at 2800-
48 3800 cm^{-1} , resulting in water stretching bands (e.g., Ratcliffe and Irish, 1982; Sun, 2009;
49 Walrafen et al., 1986). In salty solutions or brines, halogen ions interact with the bonds of water
50 molecules. Although ions and ionic bonding cannot be directly detected with Raman
51 spectroscopy, their impact on the network of covalent water bonding is detectable. This effect
52 has been the subject of numerous studies, with a substantial focus on chlorine (e.g., Dubessy
53 et al., 2002; Durickovic et al., 2010; Georgiev et al., 1984; Mernagh and Wilde, 1989;
54 Pankrushina et al., 2020; Sun, 2012; Sun et al., 2010; Tepstra et al., 1990) and, to a lesser
55 extent, on the heavy halogen bromine (e.g., Tepstra et al., 1990). Halogen anions widen the
56 water bonding network, forcing the network to change its bonding structure by favoring a
57 certain type of bonding over others. A shift in water bands can be observed, correlating with
58 the number of dissolved halogens and facilitating the determination of salt concentration in the
59 solution or in mineral fluid inclusions (e.g., Dubessy et al., 2002; Durickovic et al., 2010;
60 Georgiev et al., 1984; Mernagh and Wilde, 1989; Pankrushina et al., 2020; Sun, 2012; Sun et
61 al., 2010; Tepstra et al., 1990).

62 The heavy halogens bromine and iodine possess a larger ionic size than chlorine. Their anions
63 stretch the water network as much or even more than chlorine, causing a more pronounced
64 alteration of the Raman shift (Tepstra et al., 1990). The impact of the cations (e.g., calcium,
65 magnesium, sodium, potassium) in a salty solution seem to be negligible (Sun et al., 2010).

66 Two other factors can alter the shape of Raman water bands: (1) temperature (e.g.,
67 Krishnamurthy et al., 1983; Ratcliffe and Irish, 1982) and (2) pressure (Romanenko et al.,
68 2018). Increasing temperature has a similar effect to increasing halogen concentrations,
69 enhancing the resulting peak at around 3430 cm^{-1} . Pressure shifts the bands in the opposing
70 direction: It decreases the peak at 3430 cm^{-1} and increases the peak at 3240 cm^{-1} .

71 While fluid inclusions in minerals are typically studied at ambient temperature and its effect
72 can be ignored, the pressure in mineral fluid inclusions, such as those in quartz, is likely to be
73 elevated, potentially impacting the Raman spectrum. In this study, we present a novel
74 experimental dataset examining the impact of all three heavy halogens — chlorine, bromine,
75 and iodine — on Raman water bands concerning pressure and halogen concentration at room
76 temperature. We further compare our results to some natural fluid inclusion samples from other
77 studies to demonstrate and constrain the impact of our dataset on natural fluid inclusions.

78

79 2. Experimental setup and methods

80 Various concentrations of NaCl, NaBr, or NaI salts were dissolved in water to synthesize salty
81 solutions as starting materials (Table 1). Sodium-halogen salts exhibit excellent solubility in
82 water, and sodium serves as the dominant cation in seawater-related fluids. Despite the
83 seemingly negligible impact of cations (Sun et al., 2010), sodium was selected as the cation
84 for all three halogens to mitigate cation effects and focus on the influence of the three halogen
85 anions.

86 The experiments were conducted using a Chervin-type hydrothermal diamond anvil cell
87 (HDAC) with a pressure-driving membrane (Chervin et al., 1995). The HDAC was equipped

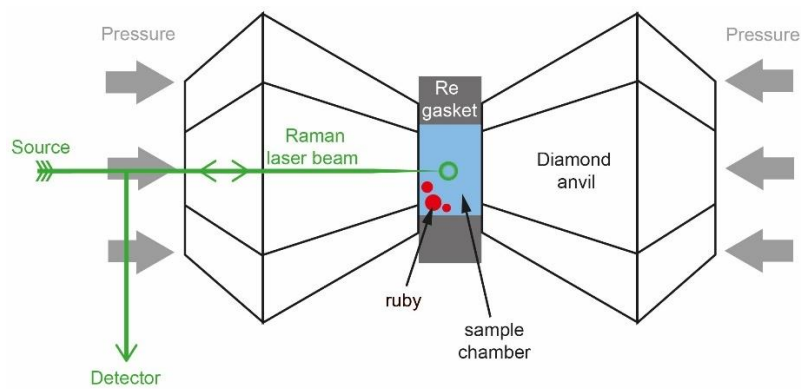
88 with 2 mm thick diamonds and culets of 1 mm diameter. The sample chamber, compressed
89 between two diamonds, had a diameter of 500 μm , drilled as a hole into a Re gasket with an
90 initial thickness of 200 μm . Before each experiment, the sample chamber was cleaned with
91 ethanol, dried, and loaded with a salty solution along with a small number of ruby spheres for
92 pressure calibration. Following HDAC closure, the membrane was connected to an inflator with
93 a N_2 gas bottle. The membrane was initially loaded with approximately 10 to 15 bar of gas
94 pressure, sufficient to seal the HDAC but insufficient to observe a fluorescence shift with the
95 ruby spheres.

96 Ruby fluorescence serves as a widely used pressure monitor for various DAC experiments
97 (e.g., Chervin et al., 2001; Shen et al., 2020). The ruby shift was calibrated with the Raman to
98 ambient pressure and had to be recalibrated for each new sample. After the ruby calibration,
99 the water bands were measured with the Raman at ambient pressure. The pressure was then
100 increased stepwise with an inflator, and pressure increases were monitored on the ruby
101 fluorescence. Pressure steps were approximately 0.2 to 0.3 GPa. Depending on the salt
102 concentration, the solution transforms into ice IV between 1.1 and 1.4 GPa (see below). After
103 each pressure increase, the cell equilibrated the pressure for about 10 minutes before Raman
104 analysis.

105 Raman measurements were performed with a 514.5 nm Argon laser and a Jobin-Yvon Horiba
106 HR460 spectrometer. A constant grating of 1500 lines/mm, a slit size of 50 μm , and a 50x
107 objective placed in front of the diamond anvil cell were used. The setup was calibrated with a
108 521 cm^{-1} silicon wafer, and the laser energy was controlled to remain constant at 10 mW
109 between each measurement during the pressure equilibration period. Diamond has no effect
110 on the Raman water bands and is widely used for these types of studies. Test runs for pure
111 water in the DAC and in a glass cylinder showed no difference in the spectra. Measurements
112 in the solution were conducted in the center of the sample chamber by defocusing the laser
113 spot between both surfaces of the two diamonds. Measurements in the solution were set for
114 10 to 30 seconds with 3 to 5 iterations. Measurements on the ruby spheres were conducted
115 "live" with a repetition rate of 1s.

116 It is important to note that halogens like iodine can also induce a Raman peak at around 1650
117 cm^{-1} (Besemer et al., 2016). However, this peak overlaps with the (extremely large) carbon
118 peak from the diamond anvils and cannot be used for hydrothermal DAC experiments or for
119 pressure calibration with HDAC.

120 The acquisition and processing of the Raman spectra were carried out using the Labspec
121 software. For baseline correction, peak deconvolution, and spectra smoothing (using "adjacent
122 averaging" with a step size of 40), the Origin software was employed. Values for R_D and S_D
123 (both are ratios that can be used to quantify the peak change numerically; see also further
124 below) were calculated prior to spectra smoothing.



125
126 *Figure 1 Experimental Setup: The saline solution was loaded into a hydrothermal*
127 *diamond anvil cell (HDAC). Pressure control was achieved using an external inflator, and*
128 *pressure levels were monitored via the fluorescence of ruby spheres suspended in the sample*
129 *chamber. Raman measurements in the solution were performed at the center of the sample*
130 *chamber by intentionally defocusing the laser spot between the surfaces of the two diamonds.*

131

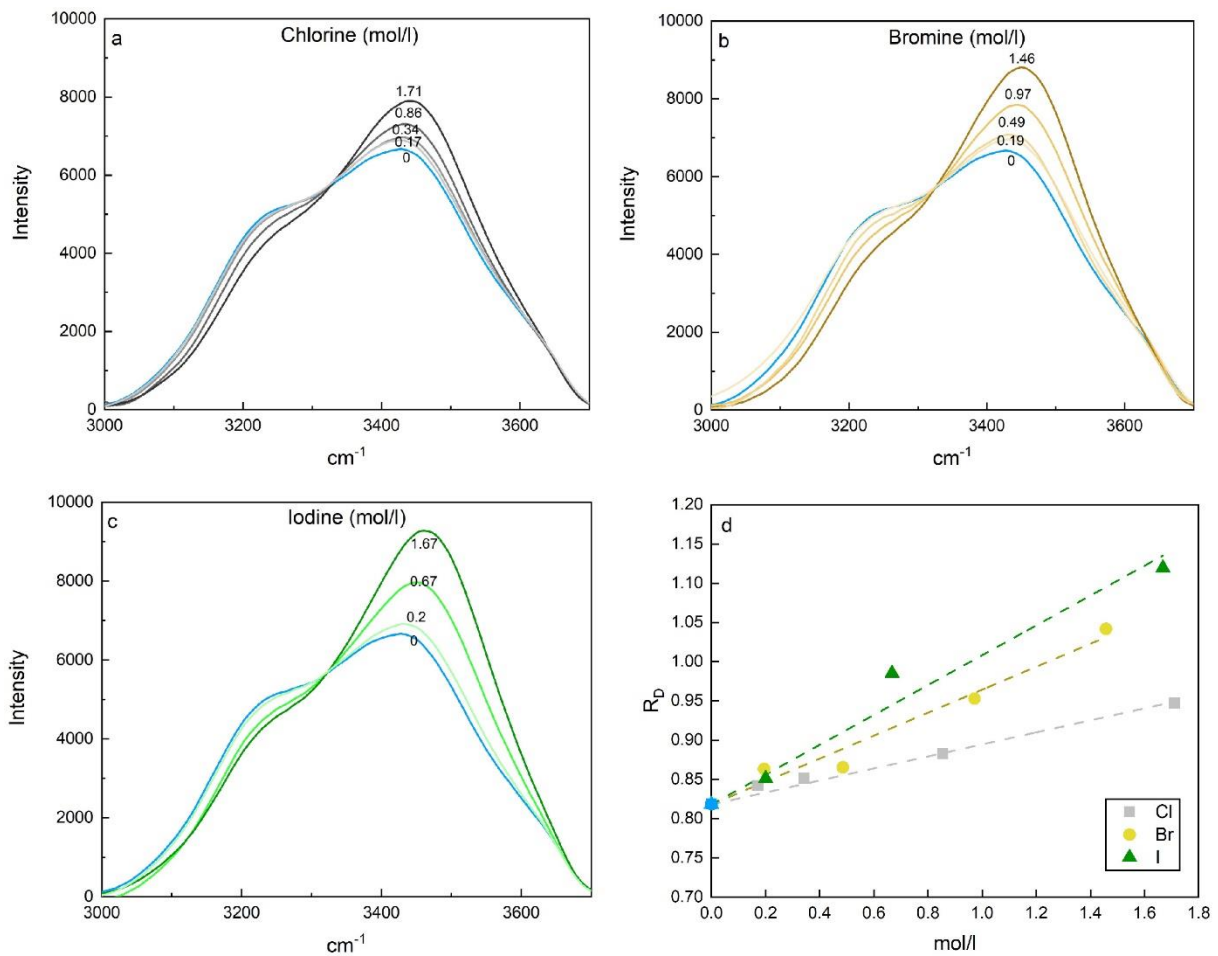
132 3. Results

133 At ambient pressure and temperature, the configuration of the water stretching bands
134 undergoes changes based on halogen concentration:

- 135 1. The 3428 cm^{-1} peak increases with rising halogen concentration: from 6660 counts for
136 pure water to 7900 counts for 1.71 mol/l chlorine, 8800 counts for 1.46 mol/l bromine, and
137 9300 counts for 1.67 mol/l iodine, respectively.
- 138 2. The 3428 cm^{-1} peak shifts to higher wavenumbers with specific positions at 3441 cm^{-1} for
139 chlorine, 3450 cm^{-1} for bromine, and 3460 cm^{-1} for iodine at their respective highest
140 concentrations.
- 141 3. The minor peak at 3240 cm^{-1} becomes relatively smaller as halogen concentration
142 increases, decreasing from 5060 counts for water to 4400 counts for chlorine, 4190 counts
143 for bromine, and 4430 counts for iodine (Figure 2).

144 At a constant halogen concentration, the characteristics of the water stretching bands evolve
145 with increasing pressure:

- 146 1. The 3428 cm^{-1} peak decreases with rising pressure: from 6975 counts at 0 GPa to 5960
147 counts at 1.1 GPa for 0.34 mol/l chlorine, from 8800 counts at 0 GPa to 7350 counts at
148 1.1 GPa for 1.45 mol/l bromine, and from 6315 counts at 0 GPa to 6010 counts at 1.39
149 GPa for 0.2 mol/l iodine.
- 150 2. The 3428 cm^{-1} peak shifts to lower wavenumbers, with new positions at 3390 cm^{-1} for
151 chlorine, from 3450 to 3435 cm^{-1} for bromine, and from 3430 to 3390 cm^{-1} for iodine at
152 their respective highest pressures.
- 153 3. The minor peak at 3240 cm^{-1} becomes relatively larger with increasing pressure, exhibiting
154 a slight increase from 4970 to 5140 counts for chlorine, from 4190 to 4590 counts for
155 bromine, and from 4960 to 5255 counts for iodine (Figure 3).



156

157 *Figure 2 The Raman water bands of saline solutions with varying concentrations of a)*
 158 *chlorine, b) bromine, and c) iodine are depicted. The halogen concentrations are indicated on*
 159 *the spectrum in mol/l. Notably, the resulting peak of the water bands at 3428 cm⁻¹ exhibits an*
 160 *increase and shifts further to the right with escalating halogen concentration. The Raman*
 161 *spectrum of pure water is represented in blue. In d), there is a discernible increase in R_D with*
 162 *escalating concentrations of chlorine, bromine, and iodine. This increase is characterized by a*
 163 *larger sum of slopes between 3325 cm⁻¹ and 3600 cm⁻¹, and a heightened peak at 3428 cm⁻¹.*
 164 *The observed effects are smallest for chlorine and most pronounced for iodine.*

165

166 4. Discussion

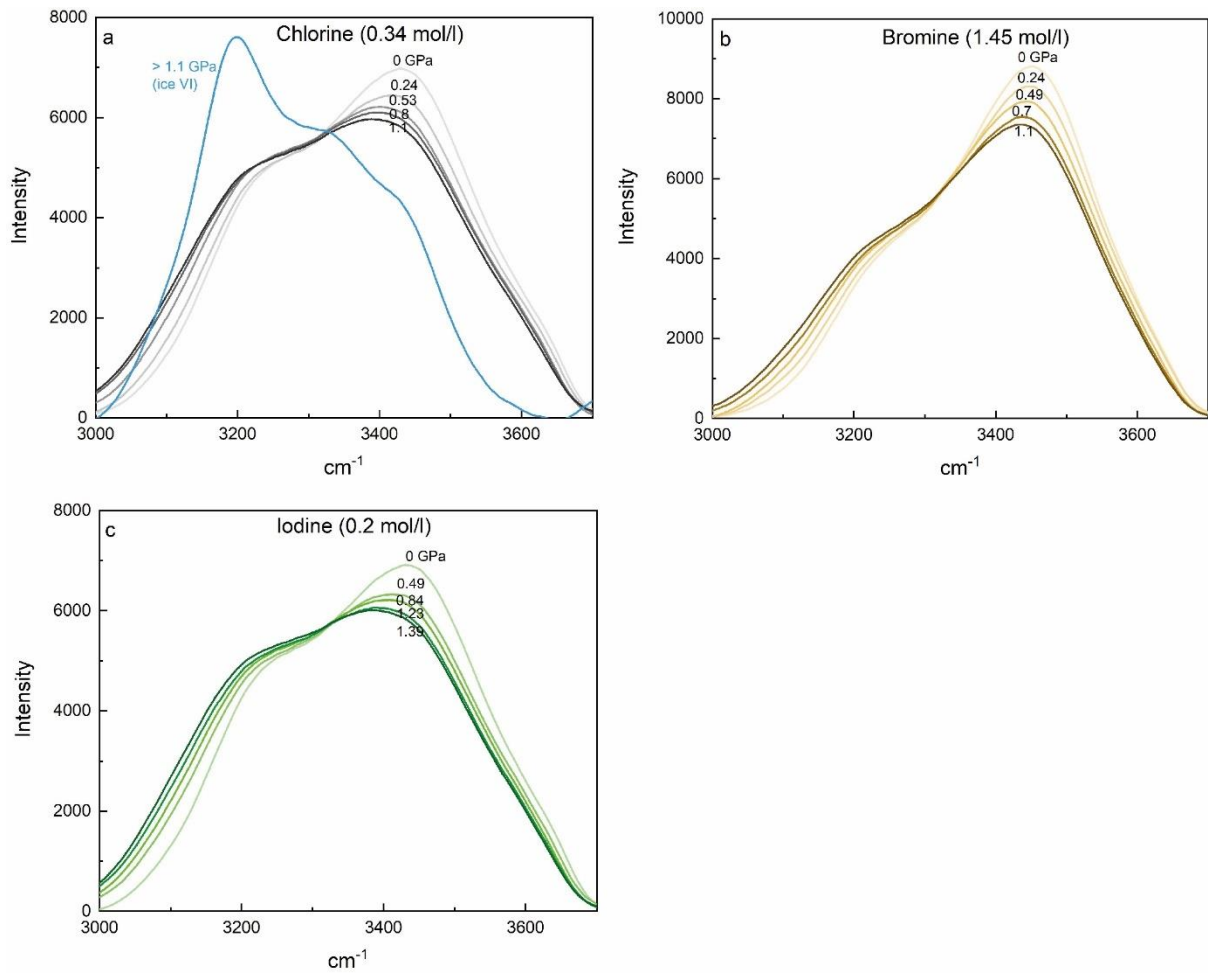
167 4.1. Halogen concentration and ionic size

168 The correlation between the change in the water bands' peak and varying halogen
169 concentration, in addition to ionic size, aligns well with findings from previous studies (Dubessy
170 et al., 2002; Durickovic et al., 2010; Georgiev et al., 1984; Mernagh and Wilde, 1989;
171 Pankrushina et al., 2020; Sun et al., 2010; Tepstra et al., 1990). The observed shift change
172 strength correlates directly with the ionic size of the halogens: Chlorine exhibits the smallest
173 shift, iodine the largest, and bromine falls in between for comparable concentrations (cf.
174 Tepstra et al., 1990 for chlorine and bromine).

175 Since ionic bonds are not Raman active, NaCl, NaBr, and NaI do not have observable modes
176 of their own, neither as salts nor as dissolved ions in water (Bakker, 2004; Pei et al., 2006;
177 Terpstra et al., 1990). Raman spectroscopy enables the observation of the vibration of
178 chemical bonds, which, in this study, is the chemical vibration of water. The halogen anions
179 are indirectly observed as they modify the vibrations of water bonding. The evolving shape of
180 the Raman spectra in Figure 2 illustrates that different halogens influence the dominant
181 bonding type in the water structure, leading to a reduction in hydrogen bonding in water. Figure
182 4 presents a deconvolution of the water stretching band into three major Gaussian components
183 representing different bonding types for water molecules:

184 Peak 1 of the first Gaussian component at 3327 cm^{-1} is attributed to 4 hydrogen bonds per
185 water molecule, involving two electron donors and two acceptors (DDAA). This peak
186 diminishes with increasing halogen content. Peak 2 at 3431 cm^{-1} is attributed to 2 hydrogen
187 bonds (DA) and becomes the predominant bonding type with increasing halogen content. Peak
188 3 at 3565 cm^{-1} is attributed to 3 hydrogen bonds per water molecule (DDA). It plays a minor
189 role in pure water as well as in salty solutions (e.g., Sun, 2009). With the addition of salt, the
190 increasing presence of cations and anions breaks the hydrogen bonds in the water network,
191 forming ionic bonds.

192 The deconvolution of the Raman water bands confirms the reduction of hydrogen bonding in
193 water with the addition of various halogens, as well as with their increasing ionic size.



194

195 *Figure 3 The Raman water bands of saline solutions are presented with fixed halogen*
 196 *concentrations and varying pressure: a) 0.34 mol/l chlorine, b) 1.45 mol/l bromine, and c) 0.2*
 197 *mol/l iodine. The pressure is indicated in GPa on the spectra. Notably, the resulting peaks*
 198 *exhibit a reduction in intensity with increasing pressure and shift towards lower wavenumbers,*
 199 *indicating a leftward shift in the spectra.*

200

201 4.2. R_D as numerical value for the changing effect

202 To quantify the changing shift of the water stretching bands, Durickovic et al. (2010) introduced
 203 the ratio S_D , defined by the formula:

204

$$S_D = \frac{\sum_{i=326}^{650} \left\{ \frac{I(i) + I(i-1)}{2} * [n(i) - n(i-1)] \right\}}{\sum_{i=1}^{325} \left\{ \frac{I(i) + I(i-1)}{2} * [n(i) - n(i-1)] \right\}}$$

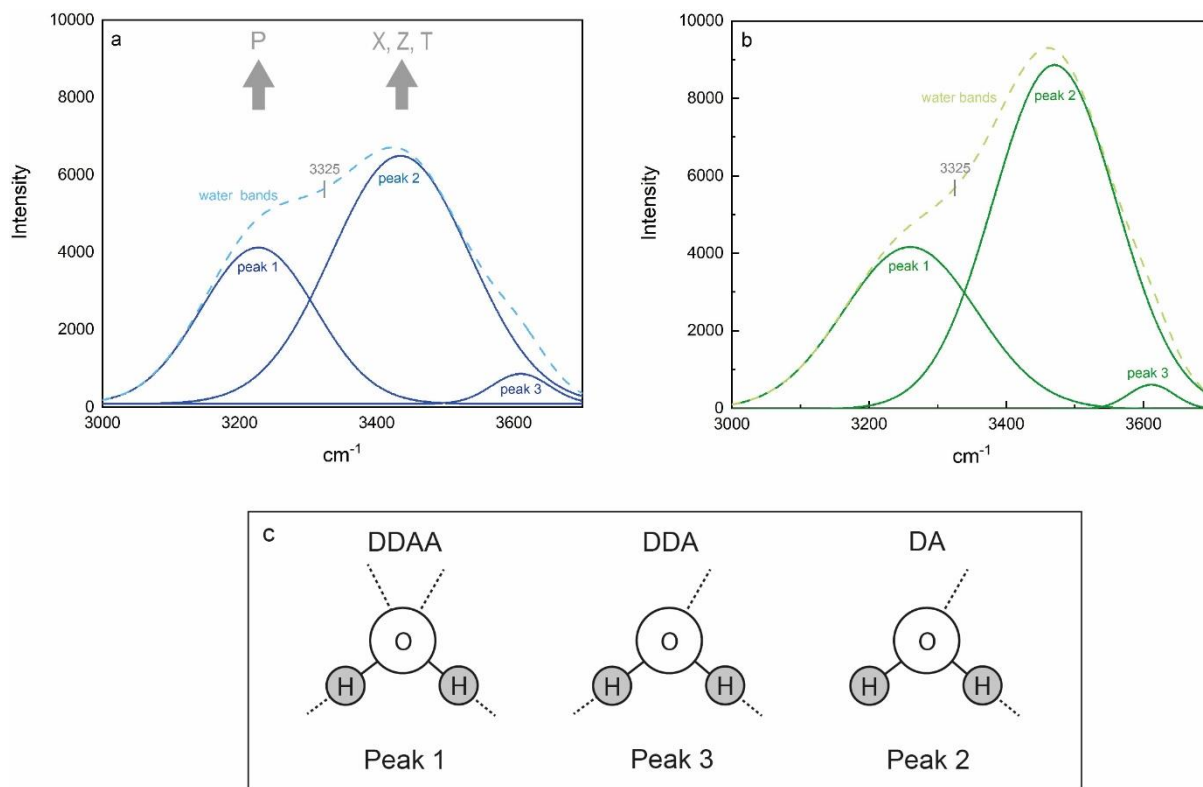
205 Here, $n(i)$ represents the shift at increment (or pixel) i , $I(i)$ is the intensity at increment (or pixel)
206 i , and the range of interest is between 3000 and 3650 cm^{-1} with a total of 650 pixels. This
207 formula establishes the inflection point of the water bands at 3325 cm^{-1} (Figure 4) and divides
208 the water bands into two halves: left and right side from the inflection point. Durickovic et al.
209 (2010) observed that S_D increases linearly with increasing NaCl concentration dissolved in
210 water.

211 With increasing halogen concentration, the slope increases on both sides of the inflection point,
212 resulting in an increase in both the sum of slopes for the left and right halves (cf., Figure 2).
213 This trend holds for all three studied halogens: chlorine, bromine, and iodine. To avoid division
214 of two values that both correlate positively and increase with higher halogen concentrations, a
215 ratio R_D was calculated, slightly different from S_D . The formula for R_D is as follows:

$$216 \quad R_D = \frac{\sum_{i=1}^{325} \left\{ \frac{I(i) + I(i-1)}{2} * [n(i) - n(i-1)] \right\}}{I_{i=1} * 325}$$

217 Here again, $n(i)$ represents the shift at increment (or pixel) i , $I(i)$ is the intensity at increment (or
218 pixel) i , and the total number of pixels considered is 325, starting from 3325 to 3650 cm^{-1} . This
219 formula reduces some information loss from S_D and steepens the slope, as both the numerator
220 and denominator of the ratio increase with increasing halogen concentration.

221 However, the applicability of R_D is limited to liquid water. R_D does not account for strong
222 changes in the shape of the slope, making it less suitable for high-pressure or low-temperature
223 polymorphs (e.g., ice VI), which exhibit the dominant peak on the left side of the inflection point
224 (Figure 3).



225

226 *Figure 4 The peak-deconvoluted Raman water bands are presented for a) pure water*
 227 *and b) 1.67 mol/l iodine, resolved into three Gaussian components. The resulting water bands*
 228 *are represented by dashed lines, with the inflection point of the water bands curve identified at*
 229 *3325 cm⁻¹. Notably, with increasing iodine content (X) halogen ionic size (Z), and temperature*
 230 *(T), peak 2 becomes larger relative to peak 1, while pressure (P) has the opposing effect. In*
 231 *c), the components of the deconvolution are explained: Peak 1 is attributed to 4 hydrogen*
 232 *bonds per water molecule, involving two electron donors and two acceptors (DDAA). Peak 2*
 233 *is attributed to 2 hydrogen bonds (DA). Peak 3 is attributed to 3 hydrogen bonds per water*
 234 *molecule (DDA) (Sun, 2009). The deconvolution of the Raman water bands confirms a*
 235 *reduction in hydrogen bonding in water with the addition of various halogens and their*
 236 *increasing ionic size. Moreover, increasing pressure correlates with an augmented number of*
 237 *hydrogen bonds.*

238

239 4.3. Pressure

240 With increasing pressure, the water stretching band peak at 3428 cm^{-1} undergoes a reduction
241 in intensity and shifts towards the left (e.g., Romanenko et al., 2018), while the smaller peak
242 at 3240 cm^{-1} experiences a slight increase. The observed change stands in contrast to the
243 effects observed during temperature increase (cf., Durickovic et al., 2010) or the addition of
244 halogens (Figure 3). This shift can be interpreted as a transition towards a higher number of
245 hydrogen bonds (from DA to DDAA) in the water molecule network (Sun, 2009, Figure 4). The
246 effect is observable for all three halogens (chlorine, bromine, and iodine) in the saline solutions
247 of this study (Figure 3).

248 Sun (2012) did not observe the pressure effect in their chlorine data and argue against its
249 existence. However, upon normalizing our data in the same way as Sun (2012), the peak at
250 3428 cm^{-1} decreases, and the water bands flatten, yet a clear pressure trend remains
251 (Supplementary Figure S1). It remains unclear why the trend was not observed in Sun (2012).

252 At pressures greater than 1 GPa and ambient temperature, water transforms into ice VI (Figure
253 3). Notably, with increasing halogen concentrations, the water-ice phase transformation shifts
254 to higher pressures. In this study, liquid water/saline solution was observed at 1.1 GPa and
255 0.34 mol/l chlorine, 1.37 GPa and 0.97 mol/l bromine, or 1.27 GPa and 0.67 mol/l iodine. The
256 experimental setup does not precisely determine if the phase boundary shifts to higher
257 pressure or if the liquid state is metastable. Journaux et al. (2013) investigated the impact of
258 NaCl on the phase boundary of ice VI and found the boundary at 1.01 GPa for 1 mol/l, 1.09
259 GPa for 2.5 mol/l, and 1.52 GPa for 4 mol/l at ambient temperature. This boundary shift is
260 much smaller than the observed range, suggesting a metastable liquid phase in our study or
261 other kinetic effects.

262 As a consequence of the pressure-related shape change of the water stretching bands, R_D
263 decreases with increasing pressure for fixed halogen concentrations (Figure 3). Figure 5
264 illustrates the R_D values vs. halogen concentration at different pressures (S_D values in
265 Supplementary Figure S2). Despite some outliers, the values follow a linear trend in the studied
266 range, as previously observed for various temperatures (Durickovic et al., 2010). Within the

267 range of comparable pressures, chlorine exhibits the lowest R_D values, while iodine
268 demonstrates the highest. Comparable trends are also observed for integrated intensities
269 (Supplementary Figure S3) but show larger scatter relative to the R_D trends in Figure 2d and
270 Figure 5.

271

272 4.4. Applications

273 4.4.1. Natural fluid inclusions with one unknown component (P or X)

274 R_D can be calculated from Raman spectra of natural fluid inclusions in minerals, as
275 demonstrated by Kawamoto et al. (2013). In their study, saline fluid inclusions in spinel-
276 harzburgite xenoliths collected from the 1991 Pinatubo pumice deposits were examined. The
277 salinity of the fluid inclusions was reported as 5.1 ± 1 wt.% NaCl equivalent (0.87 ± 0.17 mol/l),
278 measured with microthermometry. The authors employed Raman spectroscopy for qualitative
279 water measurements.

280 From the provided Raman spectrum, a R_D value of 0.79 can be calculated. The measured
281 chlorine concentration from microthermometry allows for an estimate of the pressure to be
282 around 0.5 GPa (Figure 5a). This is notably lower than the 2-3 GPa that Kawamoto and
283 colleagues estimated for the formation of the saline fluid inclusions in olivine below the
284 Pinatubo. Given the available information, it can only be speculated whether some (parts) of
285 the olivines formed at a very low pressure of 0.5 GPa, or if the inclusion lost pressure, and it
286 was not fully closed above 0.5 GPa. In this case, the inclusion could at least partially represent
287 the conditions at 0.5 GPa rather than at 2-3 GPa.

288 It is crucial to note that a fluid inclusion that closes between 810 °C and 1050 °C (Kawamoto
289 et al., 2013) will experience a decrease in pressure when cooling down to ambient
290 temperature. This phenomenon is also well observed in HDAC experiments (e.g., Bureau et
291 al., 2010, 2016; Leroy et al., 2019; Louvel et al., 2020a, 2020b) and argues for a higher
292 pressure than the 0.5 GPa that were obtained from the Raman spectrum. However, this sample

293 serves as a good illustration of how pressure can be estimated by Raman in saline fluid
294 inclusions with given salinity.

295

296 4.4.2. *Natural fluid inclusions with two unknown components (P and X)*

297 Difficulties arise when neither pressure nor salinity can be determined with a different method,
298 and only the Raman spectrum is available. This scenario may occur for fluid inclusions that
299 are too small for microthermometry, resulting in a single equation with two unknown
300 parameters that cannot be solved for a distinct value.

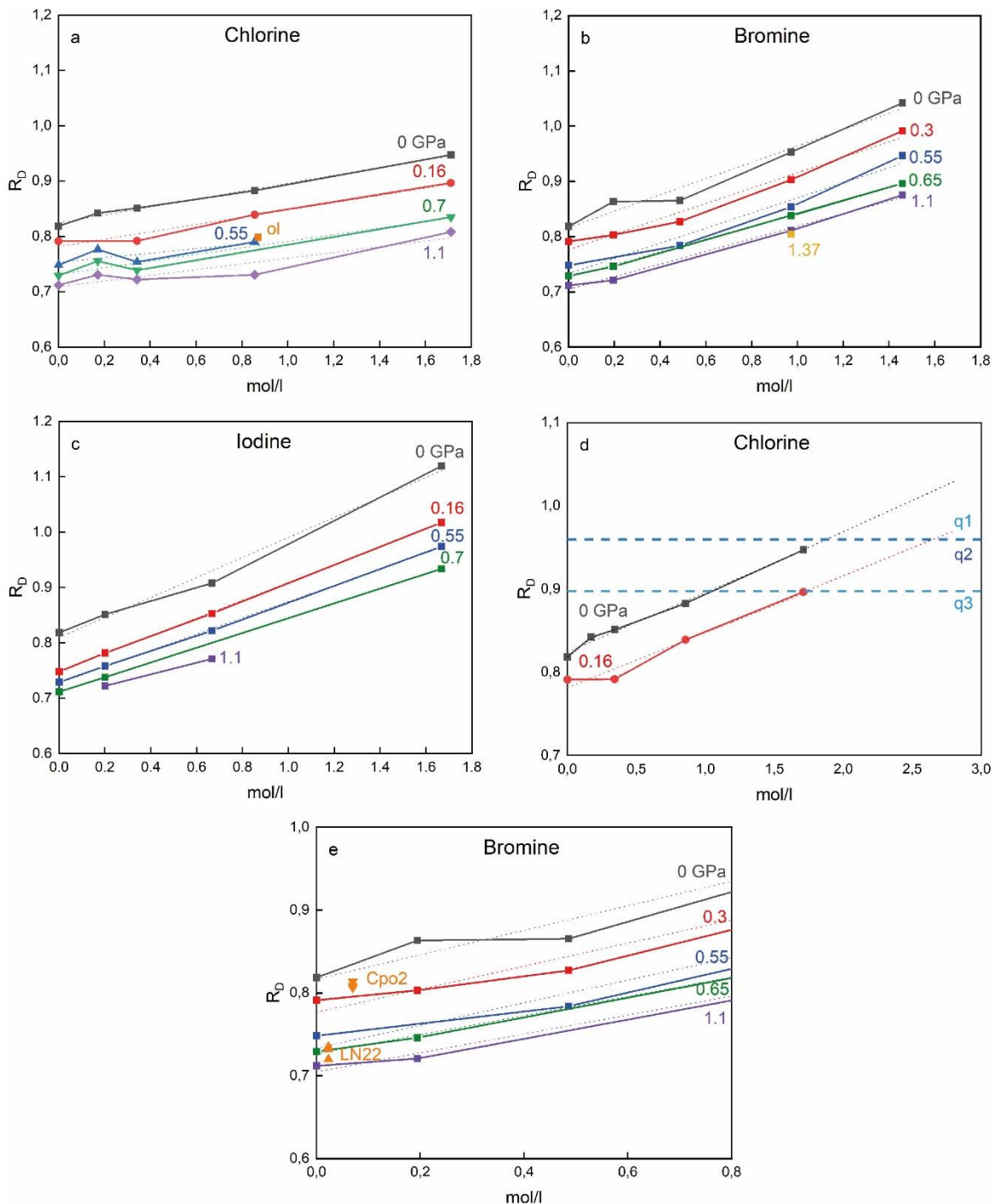
301 Saline fluid inclusions from quartz samples analyzed by Pankrushina et al. (2020) illustrate the
302 pressure dependence in Figure 5d, where R_D values plot as a constant line. For instance, q1
303 has 1.9 mol/L NaCl at ambient pressure and 2.71 mol/L at 0.16 GPa; q2 has 1.88 mol/L and
304 2.69 mol/L; and q3 has 1.02 mol/L and 1.75 mol/L at ambient pressure and at 0.16 GPa,
305 respectively. For an unknown pressure, a single salinity value cannot be determined this way.
306 Particularly at lower salinity concentrations, the range of possible salinities can be drastic: for
307 the three natural samples q1-3, a small pressure increase of 0.16 GPa changes the salinity by
308 42 to 72%. Given the stability field of quartz and saline fluids at room temperature, these are
309 conservative calculations, and a much larger pressure range of > 1 GPa must be considered.

310 However, fluid inclusions can be saturated in NaCl, and halite crystals do coexist with saline
311 fluids in the inclusion (e.g., Brooks et al., 2019). The solubility of NaCl in water at ambient P-T
312 conditions is 317 g/l or 5.4 mol/l (cf. Figure 5). The pressure effect is diminished at NaCl-
313 saturated conditions: Experiments in this study were conducted up to a salinity of 1.71 mol/L
314 for NaCl, but assuming a continuation of the observed linear trend, the difference between 0
315 and 0.16 GPa would be only 16 to 18%.

316 Therefore, the pressure effect in fluid inclusions with high salinity is smaller than in fluid
317 inclusions with low salinity. But as the potential pressure range is large (more than 1 GPa),

318 ignoring the pressure effect can lead to a huge underestimation of the salinity in the fluid, and
 319 Raman spectroscopy alone cannot be used to determine reliable salinities in fluid inclusions.

320



321

322 *Figure 5* R_D values vs halogen concentration for (a) chlorine, (b) bromine, and (c) iodine
 323 are presented in the figure. The colored lines indicate isobars: the solid lines connect the data
 324 points, while the dotted lines represent trend lines. Like the Raman water bands and the R_D

325 values, the isobars exhibit the steepest slope for high concentrations of iodine and become
326 flatter with smaller ionic halogen size, but also with increasing pressure. (a) "ol" data are from
327 a natural fluid inclusion in olivine (Kawamoto et al., 2013). (d) Calculated R_D values for natural
328 fluid inclusions in quartz demonstrate the pressure effect: q1 has 1.9 mol/L NaCl equivalent at
329 ambient pressure and 2.71 mol/L at 0.16 GPa; q2 has 1.88 mol/L and 2.69 mol/L; and q3 has
330 1.02 mol/L and 1.75 mol/L at ambient pressure and at 0.16 GPa, respectively. The fluid
331 inclusions were analyzed by Pankrushina et al. (2020) (sample names are q1 = 672; q2 =
332 33604; q3 = 20512). (e) Cpo2 and LN22 are experimental HDAC samples. Bromine content
333 was analyzed with X-ray fluorescence following the methods reported in Bureau et al. (2010)
334 and Grützner et al. (2024).

335

336 4.4.3. Heavy halogens in HDAC experiments

337 The heavy halogens bromine and iodine typically play a minor role in natural fluid inclusions.
338 The Cl/Br ratio in seawater is approximately 30, and the Cl/I ratio is around 50 (cf. Shaw and
339 Cooper, 1957 for iodine). Due to enrichment and depletion processes in the Earth's mantle,
340 Cl/Br ratios can vary significantly, ranging, for example, in diamond inclusions from 1 to 500
341 (Jonson et al., 2000). Despite their low concentration and minor role in fluid inclusions, heavy
342 halogens are highly reactive and serve as important chemical agents in Earth's atmosphere
343 (Fehn et al., 2012). Particularly for bromine, volcanoes have been recognized as significant
344 contributors (Gerlach et al., 2004), if not the primary controlling factor (Pyle and Mather, 2009),
345 to the current atmospheric content. This recognition is crucial, as bromine can be
346 approximately 60 times more efficient (Sinnhuber et al., 2009) than chlorine in the destruction
347 of stratospheric ozone (Daniel et al., 1999; Gerlach et al., 2004).

348 Over the past few decades, numerous studies have conducted high-pressure experiments on
349 bromine- and iodine-bearing fluids interacting with silica melts in hydrothermal diamond anvil
350 cells (HDAC). In these studies, the halogen content in the fluid was measured using
351 synchrotron X-ray fluorescence (Bureau et al., 2010, 2016; Kawamoto et al., 2014; Leroy et

352 al., 2019; Louvel et al., 2020a, 2020b). These experiments provide valuable insights into the
353 behavior of heavy halogens during fluid-magma degassing processes.

354 However, these experiments entail complex setups and lack reliable and easily adaptable
355 pressure sensors. The fluorescence wavelength shift of ruby is a commonly used pressure
356 sensor (e.g., Chervin et al., 2001; Shen et al., 2020), but it cannot be applied in experiments
357 conducted at elevated temperatures where ruby spheres dissolve. Other pressure indicators,
358 like X-ray diffraction of gold particles, are only reliable at higher temperatures (cf. Grützner et
359 al., 2024; Louvel et al., 2020b). Pressure monitoring in these HDAC experiments is essential
360 to understand the pressure effect on halogen partitioning between silicate melts and aqueous
361 fluids. Moreover, it is crucial to exclude pressure loss processes during the experiment (cf.
362 Bureau et al., 2010, 2016; Leroy et al., 2019; Louvel et al., 2020a, 2020b).

363 Most HDAC experiments are conducted at high temperatures, reaching several hundred
364 degrees Celsius (e.g., Bureau et al., 2010, 2016; Grützner et al., 2024; Leroy et al., 2019;
365 Louvel et al., 2020a, 2020b). The elevated temperature introduces an additional variable to the
366 shift change of the water bands, as they also change with varying temperature (Krishnamurthy
367 et al., 1983; Ratcliffe and Irish, 1982).

368 Thus far, residual pressure can be monitored at ambient temperature, for example, before and
369 after the experiment, once the fluid has been cooled down to room temperature. Figure 5e
370 illustrates two samples used for test measurements, following the experimental setup and the
371 analytical methods for bromine concentration reported in Grützner et al. (2024). These
372 samples represent experiments that tested the degassing reaction of a bromine-doped basalt
373 melt into an aqueous fluid. Experiments were conducted at high temperatures (above the
374 basalt solidus) and pressures of up to 1.7 GPa in a hydrothermal diamond anvil cell (cf.
375 Grützner et al., 2024, for a detailed description of the experiments). Bromine concentrations of
376 0.07 mol/L for sample LN22 and 0.023 mol/L for Cpo2 were measured in the fluid by
377 synchrotron x-ray fluorescence (SXRF) during the experiments. Raman spectra of the aqueous
378 fluids were analyzed after the experiment under room temperature conditions. Bromine

379 concentrations from SXRF, together with the Raman spectra, allow estimating pressure ranges
380 of 0.7 to 0.9 GPa for LN22 and 0.1 to 0.2 GPa for Cpo2. These promising results show that
381 Raman water bands can be used as pressure or salinity indicators from room to high
382 temperatures, providing additional pressure-concentration-related temperature calibrations
383 are performed.

384

385 5. Conclusion

386 Our new experimental dataset demonstrates that the impact of halogens on the change of
387 Raman water band shifts increases with ionic size from chlorine over bromine to iodine. To
388 address and compare these changes, we calculated the numerical value R_D . Our experiments
389 further show that increased pressure diminishes the impact of the halogen shift change to a
390 different extent for each of the three halogens. This can have drastic consequences for the
391 salinity calculation of fluid inclusions in minerals like quartz or olivine. Especially in the range
392 of low salinity, the concentration can be strongly underestimated if the pressure effect is
393 ignored. Either pressure or salinity needs to be determined by an independent method. For
394 experiments performed in diamond anvil cells with halogens in aqueous fluids, the change of
395 Raman water band shifts can be a beneficial (with some restrictions) tool to monitor the
396 pressure at room temperature, if salinity is known, and inversely this change can be used to
397 monitor the salinity.

398

399 6. Acknowledgments

400 This project was funded by the ANR Projet de Recherche Collaborative VOLC-HAL-CLIM
401 (Volcanic Halogens: from Deep Earth to Atmospheric Impacts), ANR-18-CE01-0018 (Hélène
402 Bureau). Tobias Grützner is grateful for the EU Marie Skłodowska-Curie Fellowship “ExCliso”
403 (Project ID 101017762). We thank K. Béneut for his support with the Raman laser we used
404 for our experiments at the IMPMC and Y. Guarnelli for his help with the DAC alignment. We

405 are very grateful to E.A. Pankrushina for providing the raw dataset of Raman spectra from
406 her study. We thank the two reviewers for their helpful comments to improve the manuscript
407 and editor Claudia Romano is thanked for handling the manuscript.

408

409

410 Statement: During the preparation of this work the authors used ChatGPT 3.5 to correct
411 errors of spelling, punctuation, grammar and to improve the syntax in several chapters of the
412 manuscript. After using this tool, the authors reviewed and edited the content and take full
413 responsibility for the content of the publication.

414

415 7. References

- 416 Aiuppa, A., Baker, D.R., & Webster, J.D., 2009. Halogens in volcanic systems. *Chem. Geol.*,
417 **263(1-4)**, 1-18. <https://doi.org/10.1016/j.chemgeo.2008.10.005>.
- 418 Bakker, R.J., 2004. Raman spectra of fluid and crystal mixtures in the systems H₂O, H₂O-NaCl
419 and H₂O-MgCl₂ at low temperatures: applications to fluid-inclusion research. *Can. Mineral.*
420 **42**, 1283-1314. <https://doi.org/10.2113/gscanmin.42.5.1283>.
- 421 Besemer, M., Bloemenkamp, R., Ariese, F., van Manen, H.-J., 2016. Identification of multiple
422 water-iodide species in concentrated NaI solutions based on the raman bending vibration of
423 water. *J. Phys. Chem. A* **120(5)**, 709-714. <https://doi.org/10.1021/acs.jpca.5b10102>.
- 424 Brooks, H.L., Dragovic, B., Lamadrid, H.M., Caddick, M.J., Bodnar, R.J., 2019. Fluid capture
425 during exhumation of subducted lithologies: A fluid inclusion study from Sifnos, Greece.
426 *Lithos* **332-333**, 120-134. <https://doi.org/10.1016/j.lithos.2019.01.014>.
- 427 Bureau, H., Keppler, H., and Métrich, N., 2000. Volcanic degassing of bromine and iodine:
428 Experimental fluid/melt partitioning data and applications to stratospheric chemistry: *Earth*
429 *Planet. Sci. Lett.* **183**, 51-60. [https://doi.org/10.1016/S0012-821X\(00\)00258-2](https://doi.org/10.1016/S0012-821X(00)00258-2).
- 430 Bureau, H., Foy, E., Raepsaet, C., Somogyi, A., Munsch, P., Simon, G., Kubsky, S., 2010.
431 Bromine cycle in subduction zones through in situ Br monitoring in diamond anvil cells.
432 *Geochim. Cosmochim. Acta* **74**, 3839–3850. <https://doi.org/10.1016/j.gca.2010.04.001>.
- 433 Bureau, H., Auzende, A.-L., Marocchi, M., Raepsaet, C., Munsch, P., Testemale, D., Mézouar,
434 M., Kubsky, S., Carrière, M., Ricolleau, A., Fiquet, G., 2016. Modern and past volcanic
435 degassing of Iodine. *Geochim. Cosmochim. Acta* **173**, 114–125.
436 <https://doi.org/10.1016/j.gca.2015.10.017>.
- 437 Chervin, J.C, Canny B., Besson, J. M., Pruzan, P., 1995. A diamond anvil cell for IR
438 microspectroscopy. *Rev. Sci. Instrum.* **66** (3), 2595-2598. <https://doi.org/10.1063/1.1145594>.

439 Chervin J.C., Canny B., Mancinelli M., 2001. Ruby-spheres as pressure gauge for optically
440 transparent high pressure cells. *High Press. Res.* **21**, 305–314.
441 <https://doi.org/10.1080/08957950108202589>.

442 Daniel, J.S., Solomon, S., Portmann, R.W., 1999. Stratospheric ozone destruction: The
443 importance of bromine relative to chlorine. *J. Geophys. Res.* **104**, 23871-23880.
444 <https://doi.org/10.1029/1999JD900381>.

445 Dubessy J., Lhomme, T., Boiron, M-C., Rull, F., 2002. Determination of Chlorinity in Aqueous
446 Fluids Using Raman Spectroscopy of the Stretching Band of Water at Room Temperature:
447 Application to Fluid Inclusions. *Appl. Spectrosc.* **56(1)**, 99-106.

448 Đuričković, I., Marchetti, M., Claverie, R., Bourson, P., Chassot, J-M., Fontana, M.D., 2010.
449 Experimental study of NaCl aqueous solutions by Raman spectroscopy: Towards a new
450 optical sensor. *Appl. Spectrosc.* **64(8)**, 853-857.
451 <https://doi.org/10.1366/000370210792080984>.

452 Fehn, U., 2012. Tracing crustal fluids: Applications of natural ¹²⁹I and ³⁶Cl. *Annu. Rev. Earth
453 Planet. Sci.* **40**, 45-67. <https://doi.org/10.1146/annurev-earth-042711-105528>.

454 Georgiev, G.M., Kalkanjiev, T.K., Petrov, V.P., Nickolov, Zh., 1984. Determination of Salts in
455 Water Solutions by a Skewing Parameter of the Water Raman Band. *Appl. Spectrosc.* **38(4)**,
456 593-595. <https://doi.org/10.1366/0003702844555106>.

457 Gerlach, T.M., 2004. Volcanic source of tropospheric ozone-depleting trace gases. *Geochem.
458 Geophys. Geosyst.* **5**, Q09007. <https://doi.org/10.1029/2004GC000747>.

459 Grützner, T., Bureau, H., Boulard, E., Munsch, P., Guignot, N., Siebert, J., Guarnelli, Y., 2024.
460 An in-situ experimental HP/HT study on bromine release from a natural basalt. *Chem. Geol.*
461 **644**, 121869. <https://doi.org/10.1016/j.chemgeo.2023.121869>.

462 Johnson, L.H., Burgess, R., Turner, G., Milledge, H.J., Harris, J.W. 2000. Noble gas and
463 halogen geochemistry of mantle fluids: comparison of African and Canadian diamonds.
464 *Geochim. Cosmochim. Acta* **64**, 717-732. [https://doi.org/10.1016/S0016-7037\(99\)00336-1](https://doi.org/10.1016/S0016-7037(99)00336-1).

465 Journaux, B., Daniel, I., Caracas, R., Montagnac, G., Cardon, H., 2013. Influence of NaCl on
466 ice VI and ice VII melting curves up to 6 GPa, implications for large icy moons. *Icarus* **226**,
467 355-363. <https://doi.org/10.1016/j.icarus.2013.05.039>.

468 Kawamoto, T., Yoshikawa, M., Kumagai, Y., Mirabueno, M.H.T., Okuno, M., Kobayashi, T.,
469 2013. Mantle wedge infiltrated with saline fluids from dehydration and decarbonation of
470 subducting slab. *Proc. Nat. Acad. Sci. USA.*, **110(24)**, 9663-9668.
471 <https://doi.org/10.1073/pnas.1302040110>.

472 Kawamoto, T., Mibe, K., Bureau, H., Reguer, S., Mocuta, C., Kubsy, S., Thiaudière, D., Ono,
473 S., Kogiso, T., 2014. Large-ion lithophile elements delivered by saline fluids to the sub-arc
474 mantle. *Earth Planets Space* **66**, 61. <https://doi.org/10.1186/1880-5981-66-61>.

475 Krishnamurthy, S., Bansil, R., Wiafe-Akente, J., 1983. Low-frequency Raman spectrum of
476 supercooled water. *J. Chem. Phys.* **79**, 5863-5870. <https://doi.org/10.1063/1.445756>.

477 Leroy, C.; Bureau, H., Sanloup, C., Raepsaet, C., Glazirin, K., Munsch, P., Harmand, M.,
478 Prouteau, G., Khodja, H., 2019. Xenon and iodine behaviour in magmas. *Earth. Planet. Sci.*
479 *Lett.* **522**, 144-154. <https://doi.org/10.1016/j.epsl.2019.06.031>.

480 Louvel, M., Cadoux, A., Brooker, R.A., Proux, O., Hazemann, J-L., 2020a. New insights on Br
481 speciation in volcanic glasses and structural controls on halogen degassing. *Am. Min.* **105**,
482 795-802. <https://doi.org/10.2138/am-2020-7273>.

483 Louvel, M., Sanchez-Valle, C., Malfait, W.J., Pokrovski, G.S., Borca, C.N., Grolimund, D.,
484 2020b. Bromine speciation and partitioning in slab-derived aqueous fluids and silicate melts
485 and implications for halogen transfer in subduction zones. *Solid Earth* **11**, 1145-1161.
486 <https://doi.org/10.5194/se-11-1145-2020>.

487 Mernagh, T.P., Wilde, A.R., 1989. The use of the laser Raman microprobe for the
488 determination of salinity in fluid inclusions. *Geochim. Cosmochim. Acta* **53(4)**, 765-771.
489 [https://doi.org/10.1016/0016-7037\(89\)90022-7](https://doi.org/10.1016/0016-7037(89)90022-7).

490 Moncada, D., Bodnar, R.J., 2012. Raman spectroscopy technique to determine the salinity of
491 fluid inclusions, PACROFI-XI (Pan-American Current Research on Fluid Inclusions)
492 Conference, pp. 67.

493 Ni, P., Ding, J., Rao, B., 2006. In situ cryogenic Raman spectroscopic studies on the synthetic
494 fluid inclusions in the systems H₂O and NaCl-H₂O. *Chin. Sci. Bull.* **51(1)**, 108-114.
495 <https://doi.org/10.1007/s11434-004-0256-5>.

496 Pankrushina, E.A., Krupenin, M.T., Shchapova, Y.V., Kobuzov, A.S., Garaeva, A.A., Votyakov,
497 S.L., 2020. The study of fluid inclusion salinity in minerals by raman spectroscopy revisited.
498 In: Votykov, S., Kiseleva, D., Grokhovsky, V., Shchapova, J. (eds.), *Minerals: Structure,*
499 *Properties, Methods of Investigation: Proceedings of the 10th All-Russian Youth Scientific*
500 *Conference* (pp. 175-183). Springer International Publishing. <https://doi.org/10.1007/978-3->
501 [030-49468-1_23](https://doi.org/10.1007/978-3-030-49468-1_23).

502 Pyle, D.M., Mather, T.A., 2009. Halogens in igneous processes and their fluxes to the
503 atmosphere and oceans from volcanic activity: A review. *Chem. Geol.* **263**, 110-121.
504 <https://doi.org/10.1016/j.chemgeo.2008.11.013>.

505 Ratcliffe, C.I., Irish, D.E., 1982. Vibrational spectral studies at elevated temperatures and
506 pressures. Raman studies of liquid water up to 300 °C. *J. Phys. Chem.* **86**, 4897-4905.
507 <https://doi.org/10.1021/j100222a013>.

508 Romanenko, A.V., Rashchenko S.V., Goryainov, S.V., Likhacheva
509 <https://doi.org/10.1177/0003702817752487>, A.Y., Korsakov, A.V., 2018. In Situ Raman
510 Study of Liquid Water at High Pressure. *Appl. Spectrosc.* **72(6)**, 847-852.
511 <https://doi.org/10.1177/0003702817752487>.

512 Shaw, T., Cooper, L., 1957. State of Iodine in Sea Water. *Nature* **180**, 250.
513 <https://doi.org/10.1038/180250a0>.

514 Shen, G., Wang, Y., Dewaele, A., Wu, C., Fratanduono, D.E., Eggert, J., Klotz, S., Dziubek,
515 K.F., Loubeyre, P., Fat'yanov, O.V., Asimov, P.D., Mashimo, T., Wentzcovitch, R.M.M., 2020.

516 Toward an international practical pressure scale: A proposal for an IPPS ruby gauge (IPPS-
517 Ruby2020). *High Press. Res.* **40(3)**, 299-314.
518 <https://doi.org/10.1080/08957959.2020.1791107>.

519 Sinnhuber, B.-M., Sheode, N., Sinnhuber, M., Chipperfield, M.P., Feng, W., 2009. The
520 contribution of anthropogenic bromine emissions to past stratospheric ozone trends: A
521 modelling study, *Atmos. Chem. Phys.*, **9(8)**, 2863-2871. [https://doi.org/10.5194/acp-9-2863-](https://doi.org/10.5194/acp-9-2863-2009)
522 2009.

523 Sun, Q., 2009. The Raman OH stretching bands of liquid water. *Vib. Spectrosc.* **51**, 213-217.
524 <https://doi.org/10.1016/j.vibspec.2009.05.002>.

525 Sun, Q., 2012. Raman spectroscopic study of the effects of dissolved NaCl on water structure.
526 *Vib. Spectrosc.* **62**, 110-114. <https://doi.org/10.1016/j.vibspec.2012.05.007>.

527 Sun, Q., Zhao, L., Li, N., Liu, J., 2010. Raman spectroscopic study for the determination of Cl-
528 concentration (molarity scale) in aqueous solutions: Application to fluid inclusions. *Chem.*
529 *Geol.* **272(1-4)**, 55-61. <https://doi.org/10.1016/j.chemgeo.2010.02.004>.

530 Terpstra, P., Combes, D., Zwick, A., 1990. Effect of salts on dynamics of water: A Raman
531 spectroscopy study. *J. Chem. Phys.* **92**, 65-70. <https://doi.org/10.1063/1.458418>.

532 Walrafen, G.E., Fisher, M.R., Hokmabadi, M.S., Yang, W.-H., 1986. Temperature dependence
533 of the low- and high-frequency Raman scattering from liquid water. *J. Chem. Phys.* **85(12)**,
534 6970-6982. <https://doi.org/10.1063/1.451384>.

535

536

537

8. Tables

	NaCl				max(NaCl) ^a
g/l	10	20	50	100	317
mol/l	0.17	0.34	0.86	1.71	5.42
wt.%	0.99	1.96	4.76	9.09	24.07

	NaBr				max(NaBr) ^a
g/l	20	50	100	150	905
mol/l	0.19	0.49	0.97	1.46	8.80
wt.%	1.96	4.76	9.09	13.04	47.51

	NaI			max(NaI) ^a
g/l	30	100	250	1793
mol/l	0.20	0.67	1.67	11.96
wt.%	2.91	9.09	20.00	64.20

^a maximum solubility in H₂O at 20 °C and ambient pressure.

538

539 *Table 1 Salt concentration in the starting solutions and maximum solubility values.*

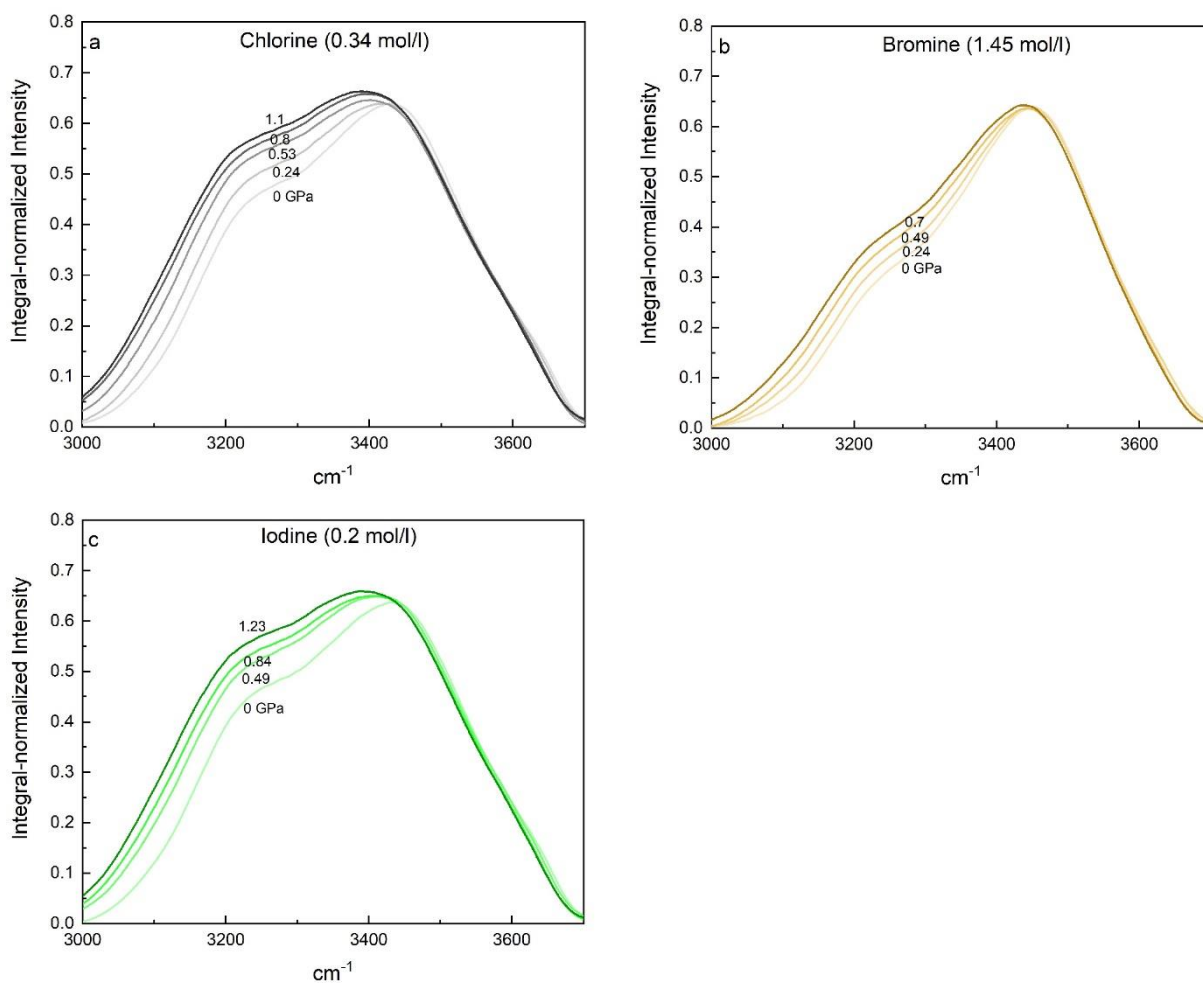
540

541

542 9. Supplementary material

543 Supplementary Tables with Raman raw data are stored under
544 <https://data.mendeley.com/datasets/tnckfpjcv/1>.

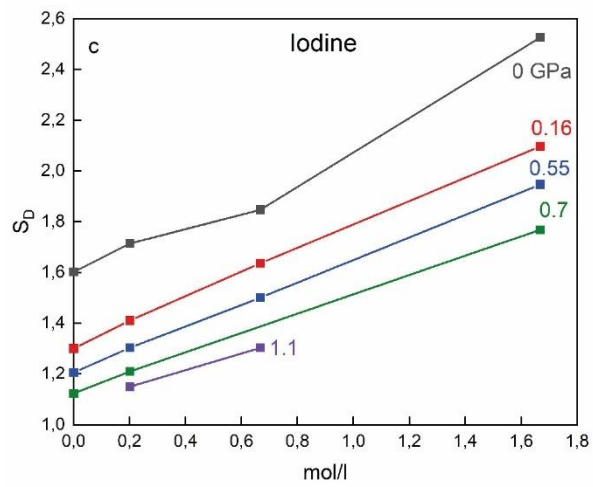
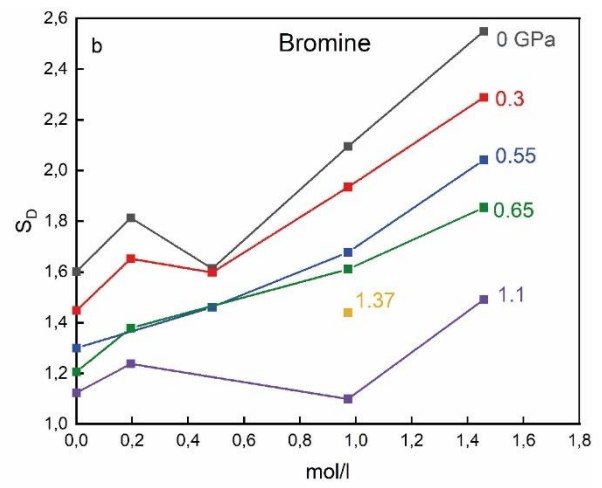
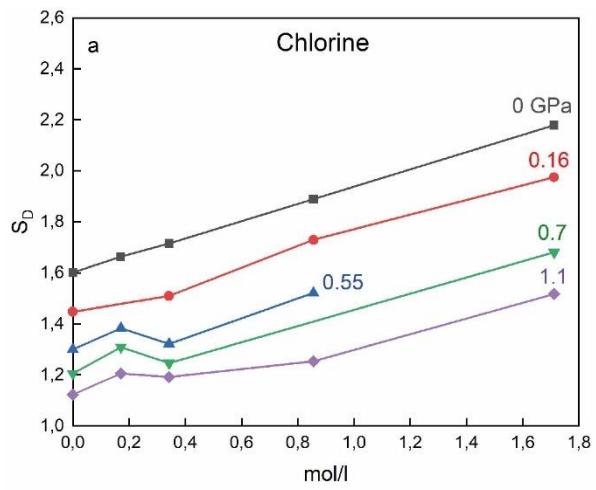
545



546

547 **Figure S1** The Raman water bands of saline solutions are presented with fixed halogen
548 concentrations and varying pressure: a) 0.34 mol/l chlorine, b) 1.45 mol/l bromine, and c) 0.2
549 mol/l iodine. The pressure is indicated in GPa on the spectra. Notably, the intensities are
550 normalized to their integrated intensities for the presented range of 3000 to 3600 cm⁻¹. The
551 resulting peaks exhibit a smaller reduction than the spectra in Figure 3 but a leftward shift in
552 the spectra indicates a clear pressure effect.

553

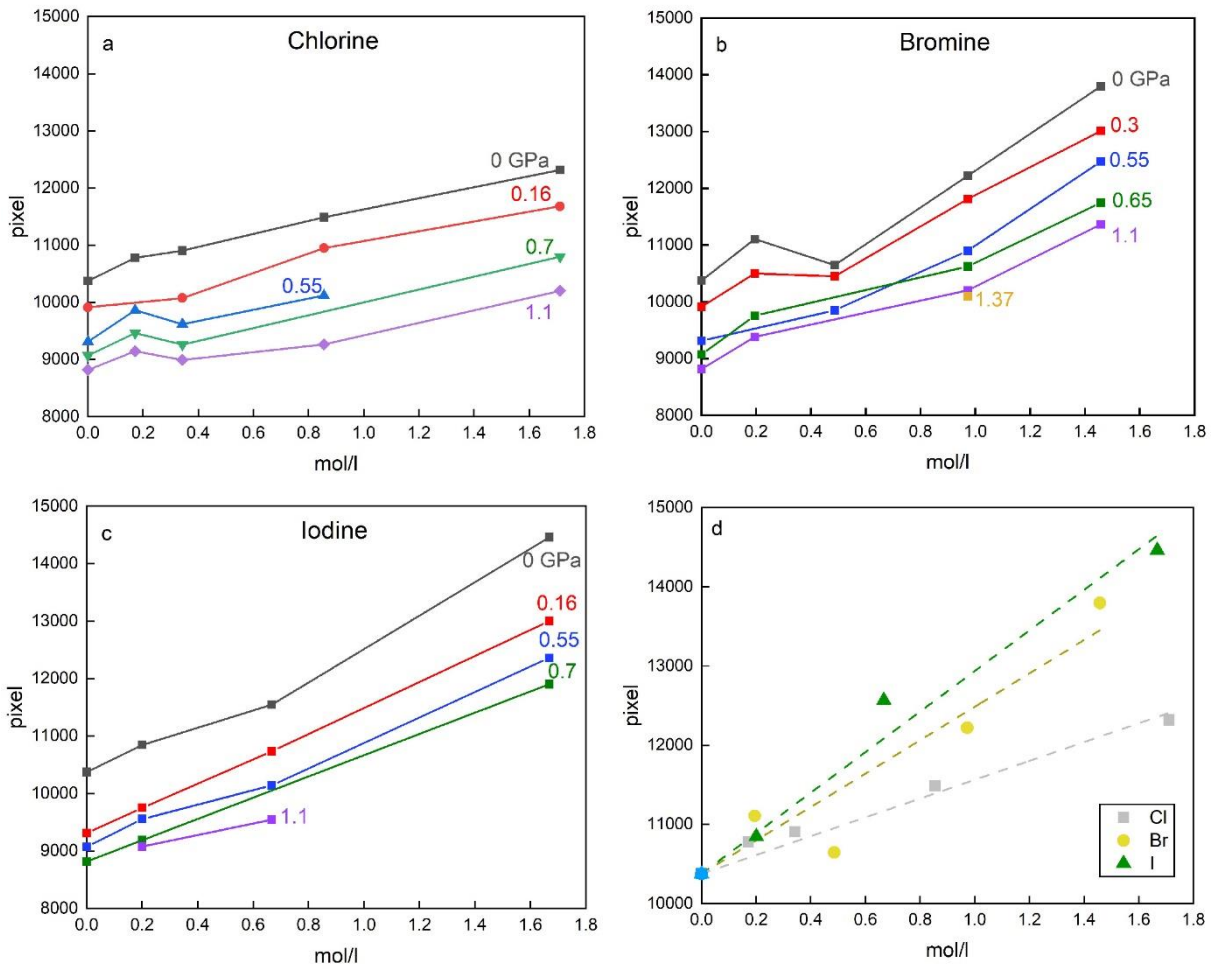


554

555 **Figure S2** S_D values vs halogen concentration for a) chlorine, b) bromine, and c) iodine

556 **calculated after Durickovic et al. (2010).**

557



558

559 **Figure S3** Integrated intensities vs halogen concentration for (a) chlorine, (b) bromine, (c)
 560 iodine, and (d) all three elements at ambient pressure show comparable trends but large
 561 scatter relative to the R_D values. The intensities were integrated over the range of 3000 to 3600
 562 cm^{-1} .

563

1 Heavy halogen impact on Raman water bands at high pressure:
2 implications for salinity estimations in fluid inclusions

3 Tobias Grützner^{1,2,3*}, Hélène Bureau¹

4

5 ¹ Institut de Minéralogie, de Physique des Matériaux et de Cosmochimie (IMPMC), Sorbonne
6 Université Paris, France.

7 ² Research School of Earth Sciences, Australian National University, Canberra, Australia.

8 ³ Institut für Geowissenschaften, Goethe-Universität Frankfurt, Germany.

9

10 *Corresponding author

11

12 Email addresses: tobias.gruetzner@outlook.com (T. Grützner), helene.bureau@sorbonne-
13 universite.fr (H. Bureau).

14

15

16 Abstract

17 We present a new experimental dataset on the impact of the heavy halogens chlorine, bromine
18 and iodine on the Raman water bands concerning pressure and their concentration at room
19 temperature. These experiments were conducted at ambient temperature, with variations in
20 halogen concentration and pressure ranging from 0 to 1.4 GPa.

21 The strength of the Raman water band shift change increases with the ionic size from chlorine,
22 over bromine, to iodine. Our experiments further demonstrate that increased pressure
23 diminishes the impact of the halogen shift change to a varying extent for each of the three
24 halogens. This finding can have significant implications for the salinity calculation of fluid
25 inclusions in minerals such as quartz or olivine. Particularly in the low salinity range, the
26 concentration can be markedly underestimated if the pressure effect is neglected. For
27 experiments in diamond anvil cells involving halogens dissolved in water, the change in Raman
28 water band shifts can serve either as a new tool to monitor pressure, or to monitor the salinity.

29

30

31 Keywords

32 Raman, water bands, Fluid inclusion, halogens, salinity, high pressure

33

34 1. Introduction

35 Halogens play a pivotal role as volatile elements, significantly impacting geodynamic
36 processes. They constitute essential components of volcanic fumaroles and volcanic ejecta.
37 Upon release into the atmosphere, halogens contribute to ozone destruction. In crustal
38 hydrothermal fluids, halogen complexes (e.g., in saline fluids, brines, or molten salts) serve as
39 major agents for metal transport in ore-forming processes related to hydrothermal systems
40 (e.g., Aiuppa et al., 2009). Samples of such fluids can be found entrapped as inclusions in
41 minerals like quartz (e.g., Brooks et al., 2019; Pankrushina et al., 2020) or olivine (e.g.,
42 Kawamoto et al., 2013) in magmatic and metamorphic rocks. Raman spectroscopy has been
43 employed for decades to determine the salinity of fluid inclusions, especially those too small
44 for other common techniques like microthermometry – a method that determines salinity by
45 observing and measuring the freezing temperature of the fluid (cf. e.g., Kawamoto et al., 2013;
46 Moncada and Bodnar, 2012; Brooks et al., 2019).

47 The Raman spectra of water and aqueous fluids exhibit several peaks closely grouped at 2800-
48 3800 cm^{-1} , resulting in water stretching bands (e.g., Ratcliffe and Irish, 1982; Sun, 2009;
49 Walrafen et al., 1986). In salty solutions or brines, halogen ions interact with the bonds of water
50 molecules. Although ions and ionic bonding cannot be directly detected with Raman
51 spectroscopy, their impact on the network of covalent water bonding is detectable. This effect
52 has been the subject of numerous studies, with a substantial focus on chlorine (e.g., Dubessy
53 et al., 2002; Durickovic et al., 2010; Georgiev et al., 1984; Mernagh and Wilde, 1989;
54 Pankrushina et al., 2020; Sun, 2012; Sun et al., 2010; Tepstra et al., 1990) and, to a lesser
55 extent, on the heavy halogen bromine (e.g., Tepstra et al., 1990). Halogen anions widen the
56 water bonding network, forcing the network to change its bonding structure by favoring a
57 certain type of bonding over others. A shift in water bands can be observed, correlating with
58 the number of dissolved halogens and facilitating the determination of salt concentration in the
59 solution or in mineral fluid inclusions (e.g., Dubessy et al., 2002; Durickovic et al., 2010;
60 Georgiev et al., 1984; Mernagh and Wilde, 1989; Pankrushina et al., 2020; Sun, 2012; Sun et
61 al., 2010; Tepstra et al., 1990).

62 The heavy halogens bromine and iodine possess a larger ionic size than chlorine. Their anions
63 stretch the water network as much or even more than chlorine, causing a more pronounced
64 alteration of the Raman shift (Tepstra et al., 1990). The impact of the cations (e.g., calcium,
65 magnesium, sodium, potassium) in a salty solution seem to be negligible (Sun et al., 2010).

66 Two other factors can alter the shape of Raman water bands: (1) temperature (e.g.,
67 Krishnamurthy et al., 1983; Ratcliffe and Irish, 1982) and (2) pressure (Romanenko et al.,
68 2018). Increasing temperature has a similar effect to increasing halogen concentrations,
69 enhancing the resulting peak at around 3430 cm^{-1} . Pressure shifts the bands in the opposing
70 direction: It decreases the peak at 3430 cm^{-1} and increases the peak at 3240 cm^{-1} .

71 While fluid inclusions in minerals are typically studied at ambient temperature and its effect
72 can be ignored, the pressure in mineral fluid inclusions, such as those in quartz, is likely to be
73 elevated, potentially impacting the Raman spectrum. In this study, we present a novel
74 experimental dataset examining the impact of all three heavy halogens — chlorine, bromine,
75 and iodine — on Raman water bands concerning pressure and halogen concentration at room
76 temperature. We further compare our results to some natural fluid inclusion samples from other
77 studies to demonstrate and constrain the impact of our dataset on natural fluid inclusions.

78

79 2. Experimental setup and methods

80 Various concentrations of NaCl, NaBr, or NaI salts were dissolved in water to synthesize salty
81 solutions as starting materials (Table 1). Sodium-halogen salts exhibit excellent solubility in
82 water, and sodium serves as the dominant cation in seawater-related fluids. Despite the
83 seemingly negligible impact of cations (Sun et al., 2010), sodium was selected as the cation
84 for all three halogens to mitigate cation effects and focus on the influence of the three halogen
85 anions.

86 The experiments were conducted using a Chervin-type hydrothermal diamond anvil cell
87 (HDAC) with a pressure-driving membrane (Chervin et al., 1995). The HDAC was equipped

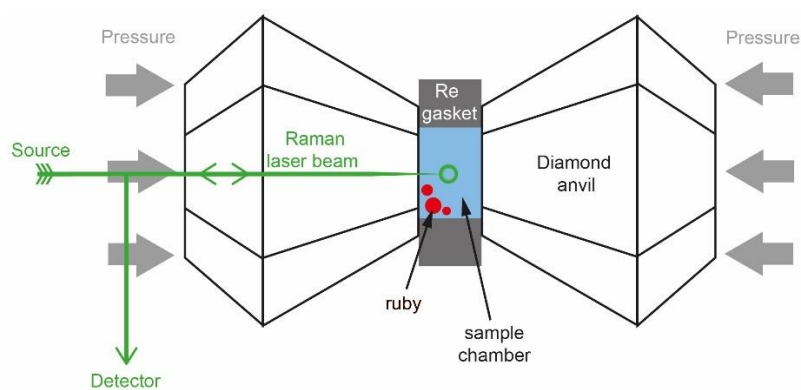
88 with 2 mm thick diamonds and culets of 1 mm diameter. The sample chamber, compressed
89 between two diamonds, had a diameter of 500 μm , drilled as a hole into a Re gasket with an
90 initial thickness of 200 μm . Before each experiment, the sample chamber was cleaned with
91 ethanol, dried, and loaded with a salty solution along with a small number of ruby spheres for
92 pressure calibration. Following HDAC closure, the membrane was connected to an inflator with
93 a N_2 gas bottle. The membrane was initially loaded with approximately 10 to 15 bar of gas
94 pressure, sufficient to seal the HDAC but insufficient to observe a fluorescence shift with the
95 ruby spheres.

96 Ruby fluorescence serves as a widely used pressure monitor for various DAC experiments
97 (e.g., Chervin et al., 2001; Shen et al., 2020). The ruby shift was calibrated with the Raman to
98 ambient pressure and had to be recalibrated for each new sample. After the ruby calibration,
99 the water bands were measured with the Raman at ambient pressure. The pressure was then
100 increased stepwise with an inflator, and pressure increases were monitored on the ruby
101 fluorescence. Pressure steps were approximately 0.2 to 0.3 GPa. Depending on the salt
102 concentration, the solution transforms into ice IV between 1.1 and 1.4 GPa (see below). After
103 each pressure increase, the cell equilibrated the pressure for about 10 minutes before Raman
104 analysis.

105 Raman measurements were performed with a 514.5 nm Argon laser and a Jobin-Yvon Horiba
106 HR460 spectrometer. A constant grating of 1500 lines/mm, a slit size of 50 μm , and a 50x
107 objective placed in front of the diamond anvil cell were used. The setup was calibrated with a
108 521 cm^{-1} silicon wafer, and the laser energy was controlled to remain constant at 10 mW
109 between each measurement during the pressure equilibration period. Diamond has no effect
110 on the Raman water bands and is widely used for these types of studies. Test runs for pure
111 water in the DAC and in a glass cylinder showed no difference in the spectra. Measurements
112 in the solution were conducted in the center of the sample chamber by defocusing the laser
113 spot between both surfaces of the two diamonds. Measurements in the solution were set for
114 10 to 30 seconds with 3 to 5 iterations. Measurements on the ruby spheres were conducted
115 "live" with a repetition rate of 1s.

116 It is important to note that halogens like iodine can also induce a Raman peak at around 1650
117 cm^{-1} (Besemer et al., 2016). However, this peak overlaps with the (extremely large) carbon
118 peak from the diamond anvils and cannot be used for hydrothermal DAC experiments or for
119 pressure calibration with HDAC.

120 The acquisition and processing of the Raman spectra were carried out using the Labspec
121 software. For baseline correction, peak deconvolution, and spectra smoothing (using "adjacent
122 averaging" with a step size of 40), the Origin software was employed. Values for R_D and S_D
123 (both are ratios that can be used to quantify the peak change numerically; see also further
124 below) were calculated prior to spectra smoothing.



125
126 *Figure 1 Experimental Setup: The saline solution was loaded into a hydrothermal*
127 *diamond anvil cell (HDAC). Pressure control was achieved using an external inflator, and*
128 *pressure levels were monitored via the fluorescence of ruby spheres suspended in the sample*
129 *chamber. Raman measurements in the solution were performed at the center of the sample*
130 *chamber by intentionally defocusing the laser spot between the surfaces of the two diamonds.*

131

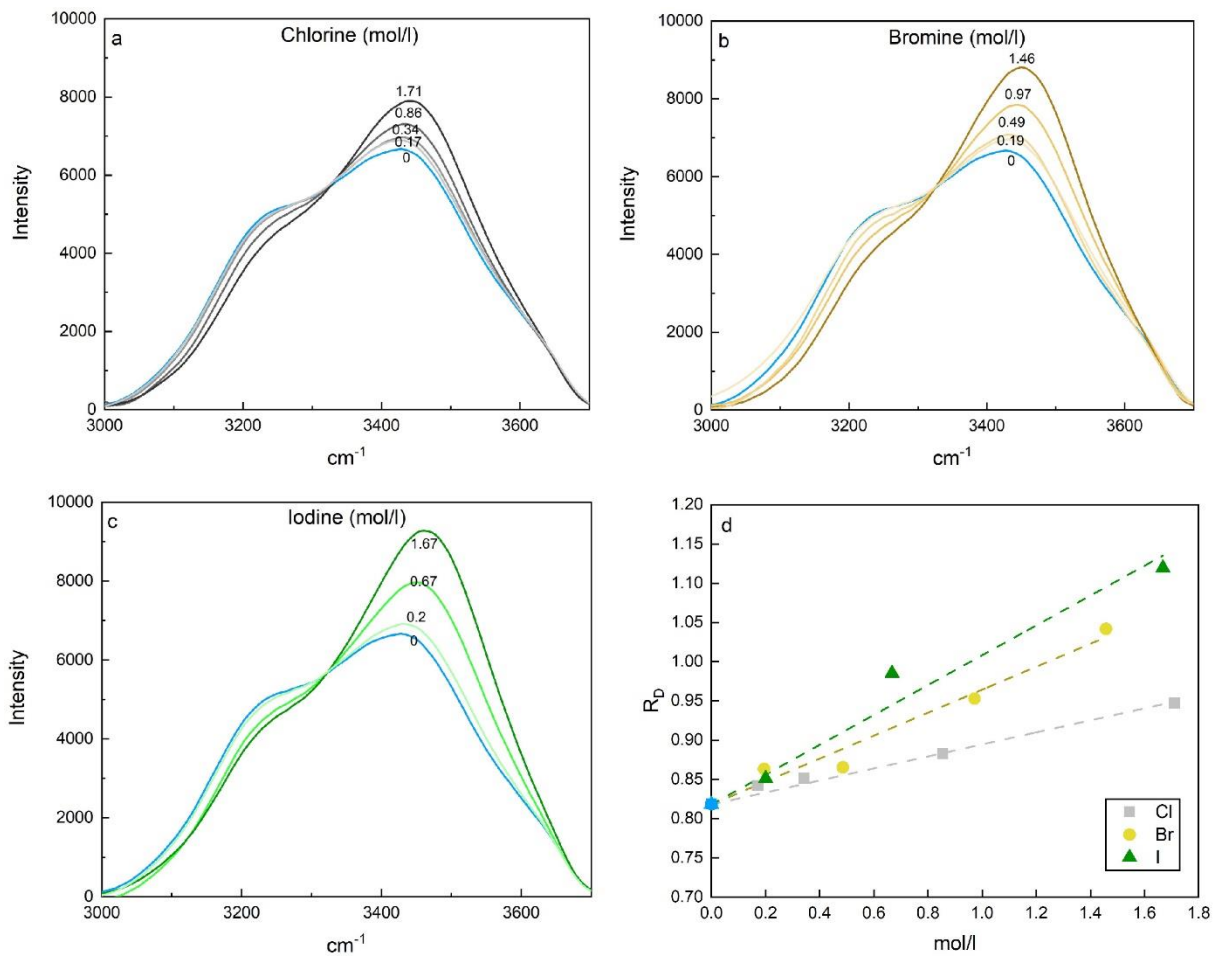
132 3. Results

133 At ambient pressure and temperature, the configuration of the water stretching bands
134 undergoes changes based on halogen concentration:

- 135 1. The 3428 cm^{-1} peak increases with rising halogen concentration: from 6660 counts for
136 pure water to 7900 counts for 1.71 mol/l chlorine, 8800 counts for 1.46 mol/l bromine, and
137 9300 counts for 1.67 mol/l iodine, respectively.
- 138 2. The 3428 cm^{-1} peak shifts to higher wavenumbers with specific positions at 3441 cm^{-1} for
139 chlorine, 3450 cm^{-1} for bromine, and 3460 cm^{-1} for iodine at their respective highest
140 concentrations.
- 141 3. The minor peak at 3240 cm^{-1} becomes relatively smaller as halogen concentration
142 increases, decreasing from 5060 counts for water to 4400 counts for chlorine, 4190 counts
143 for bromine, and 4430 counts for iodine (Figure 2).

144 At a constant halogen concentration, the characteristics of the water stretching bands evolve
145 with increasing pressure:

- 146 1. The 3428 cm^{-1} peak decreases with rising pressure: from 6975 counts at 0 GPa to 5960
147 counts at 1.1 GPa for 0.34 mol/l chlorine, from 8800 counts at 0 GPa to 7350 counts at
148 1.1 GPa for 1.45 mol/l bromine, and from 6315 counts at 0 GPa to 6010 counts at 1.39
149 GPa for 0.2 mol/l iodine.
- 150 2. The 3428 cm^{-1} peak shifts to lower wavenumbers, with new positions at 3390 cm^{-1} for
151 chlorine, from 3450 to 3435 cm^{-1} for bromine, and from 3430 to 3390 cm^{-1} for iodine at
152 their respective highest pressures.
- 153 3. The minor peak at 3240 cm^{-1} becomes relatively larger with increasing pressure, exhibiting
154 a slight increase from 4970 to 5140 counts for chlorine, from 4190 to 4590 counts for
155 bromine, and from 4960 to 5255 counts for iodine (Figure 3).



156

157 *Figure 2 The Raman water bands of saline solutions with varying concentrations of a)*
 158 *chlorine, b) bromine, and c) iodine are depicted. The halogen concentrations are indicated on*
 159 *the spectrum in mol/l. Notably, the resulting peak of the water bands at 3428 cm⁻¹ exhibits an*
 160 *increase and shifts further to the right with escalating halogen concentration. The Raman*
 161 *spectrum of pure water is represented in blue. In d), there is a discernible increase in R_D with*
 162 *escalating concentrations of chlorine, bromine, and iodine. This increase is characterized by a*
 163 *larger sum of slopes between 3325 cm⁻¹ and 3600 cm⁻¹, and a heightened peak at 3428 cm⁻¹.*
 164 *The observed effects are smallest for chlorine and most pronounced for iodine.*

165

166 4. Discussion

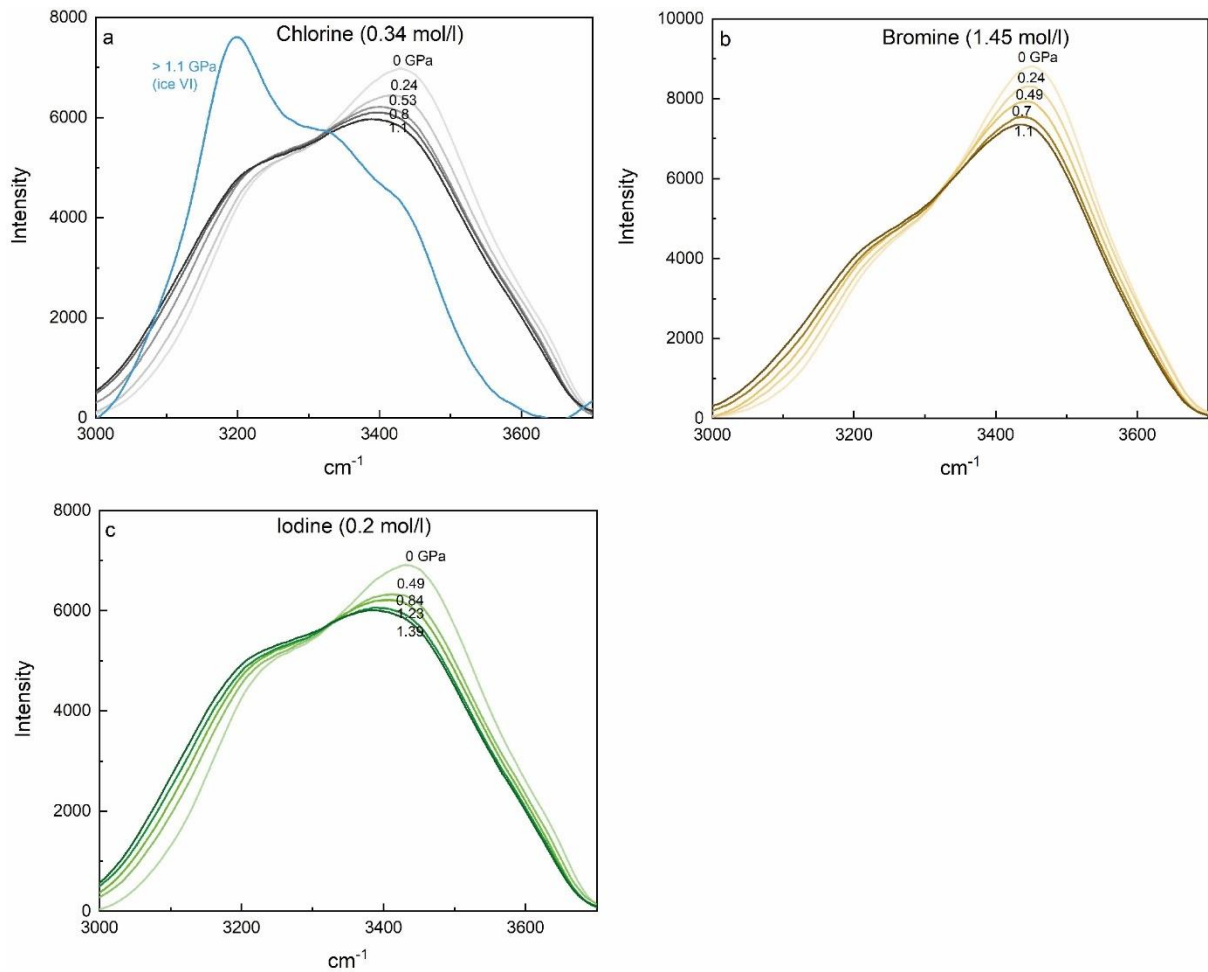
167 4.1. Halogen concentration and ionic size

168 The correlation between the change in the water bands' peak and varying halogen
169 concentration, in addition to ionic size, aligns well with findings from previous studies (Dubessy
170 et al., 2002; Durickovic et al., 2010; Georgiev et al., 1984; Mernagh and Wilde, 1989;
171 Pankrushina et al., 2020; Sun et al., 2010; Tepstra et al., 1990). The observed shift change
172 strength correlates directly with the ionic size of the halogens: Chlorine exhibits the smallest
173 shift, iodine the largest, and bromine falls in between for comparable concentrations (cf.
174 Tepstra et al., 1990 for chlorine and bromine).

175 Since ionic bonds are not Raman active, NaCl, NaBr, and NaI do not have observable modes
176 of their own, neither as salts nor as dissolved ions in water (Bakker, 2004; Pei et al., 2006;
177 Terpstra et al., 1990). Raman spectroscopy enables the observation of the vibration of
178 chemical bonds, which, in this study, is the chemical vibration of water. The halogen anions
179 are indirectly observed as they modify the vibrations of water bonding. The evolving shape of
180 the Raman spectra in Figure 2 illustrates that different halogens influence the dominant
181 bonding type in the water structure, leading to a reduction in hydrogen bonding in water. Figure
182 4 presents a deconvolution of the water stretching band into three major Gaussian components
183 representing different bonding types for water molecules:

184 Peak 1 of the first Gaussian component at 3327 cm^{-1} is attributed to 4 hydrogen bonds per
185 water molecule, involving two electron donors and two acceptors (DDAA). This peak
186 diminishes with increasing halogen content. Peak 2 at 3431 cm^{-1} is attributed to 2 hydrogen
187 bonds (DA) and becomes the predominant bonding type with increasing halogen content. Peak
188 3 at 3565 cm^{-1} is attributed to 3 hydrogen bonds per water molecule (DDA). It plays a minor
189 role in pure water as well as in salty solutions (e.g., Sun, 2009). With the addition of salt, the
190 increasing presence of cations and anions breaks the hydrogen bonds in the water network,
191 forming ionic bonds.

192 The deconvolution of the Raman water bands confirms the reduction of hydrogen bonding in
193 water with the addition of various halogens, as well as with their increasing ionic size.



194

195 *Figure 3 The Raman water bands of saline solutions are presented with fixed halogen*
 196 *concentrations and varying pressure: a) 0.34 mol/l chlorine, b) 1.45 mol/l bromine, and c) 0.2*
 197 *mol/l iodine. The pressure is indicated in GPa on the spectra. Notably, the resulting peaks*
 198 *exhibit a reduction in intensity with increasing pressure and shift towards lower wavenumbers,*
 199 *indicating a leftward shift in the spectra.*

200

201 4.2. R_D as numerical value for the changing effect

202 To quantify the changing shift of the water stretching bands, Durickovic et al. (2010) introduced
 203 the ratio S_D , defined by the formula:

204

$$S_D = \frac{\sum_{i=326}^{650} \left\{ \frac{I(i) + I(i-1)}{2} * [n(i) - n(i-1)] \right\}}{\sum_{i=1}^{325} \left\{ \frac{I(i) + I(i-1)}{2} * [n(i) - n(i-1)] \right\}}$$

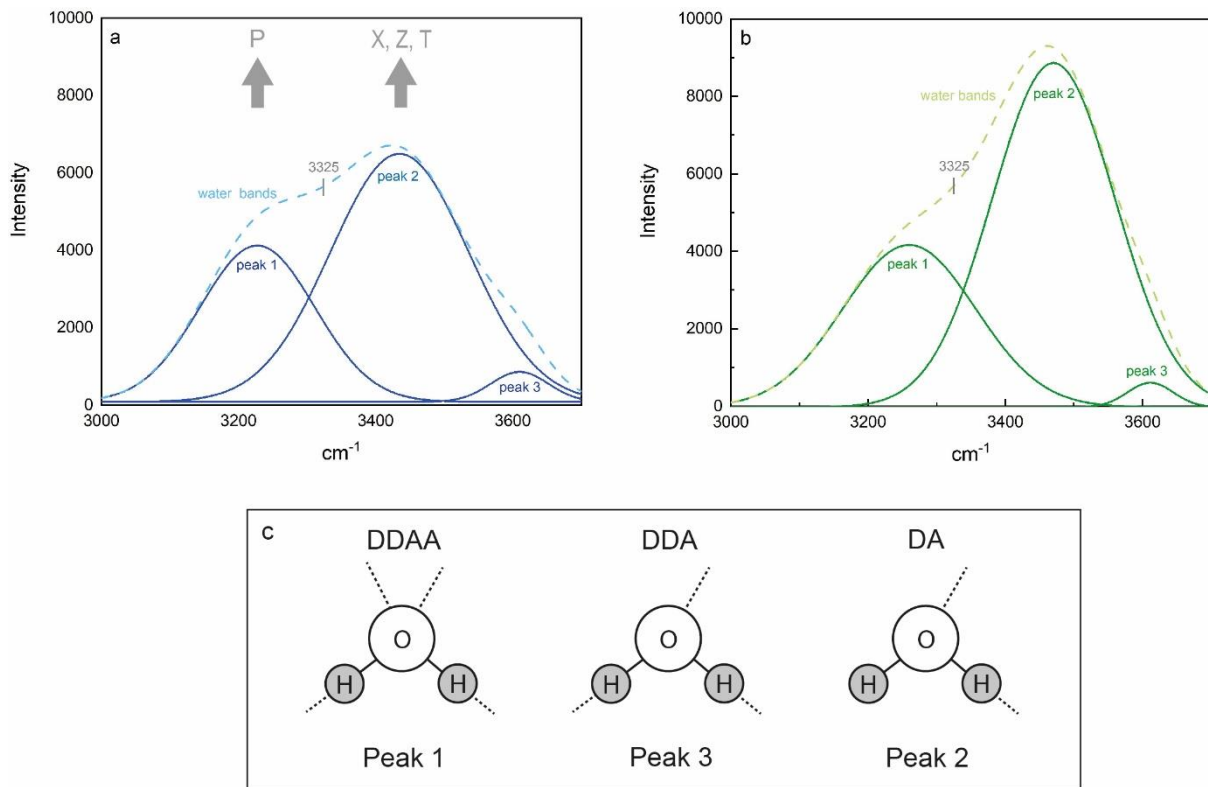
205 Here, $n(i)$ represents the shift at increment (or pixel) i , $I(i)$ is the intensity at increment (or pixel)
206 i , and the range of interest is between 3000 and 3650 cm^{-1} with a total of 650 pixels. This
207 formula establishes the inflection point of the water bands at 3325 cm^{-1} (Figure 4) and divides
208 the water bands into two halves: left and right side from the inflection point. Durickovic et al.
209 (2010) observed that S_D increases linearly with increasing NaCl concentration dissolved in
210 water.

211 With increasing halogen concentration, the slope increases on both sides of the inflection point,
212 resulting in an increase in both the sum of slopes for the left and right halves (cf., Figure 2).
213 This trend holds for all three studied halogens: chlorine, bromine, and iodine. To avoid division
214 of two values that both correlate positively and increase with higher halogen concentrations, a
215 ratio R_D was calculated, slightly different from S_D . The formula for R_D is as follows:

$$216 \quad R_D = \frac{\sum_{i=1}^{325} \left\{ \frac{I(i) + I(i-1)}{2} * [n(i) - n(i-1)] \right\}}{I_{i=1} * 325}$$

217 Here again, $n(i)$ represents the shift at increment (or pixel) i , $I(i)$ is the intensity at increment (or
218 pixel) i , and the total number of pixels considered is 325, starting from 3325 to 3650 cm^{-1} . This
219 formula reduces some information loss from S_D and steepens the slope, as both the numerator
220 and denominator of the ratio increase with increasing halogen concentration.

221 However, the applicability of R_D is limited to liquid water. R_D does not account for strong
222 changes in the shape of the slope, making it less suitable for high-pressure or low-temperature
223 polymorphs (e.g., ice VI), which exhibit the dominant peak on the left side of the inflection point
224 (Figure 3).



225

226 *Figure 4 The peak-deconvoluted Raman water bands are presented for a) pure water*
 227 *and b) 1.67 mol/l iodine, resolved into three Gaussian components. The resulting water bands*
 228 *are represented by dashed lines, with the inflection point of the water bands curve identified at*
 229 *3325 cm⁻¹. Notably, with increasing iodine content (X) halogen ionic size (Z), and temperature*
 230 *(T), peak 2 becomes larger relative to peak 1, while pressure (P) has the opposing effect. In*
 231 *c), the components of the deconvolution are explained: Peak 1 is attributed to 4 hydrogen*
 232 *bonds per water molecule, involving two electron donors and two acceptors (DDAA). Peak 2*
 233 *is attributed to 2 hydrogen bonds (DA). Peak 3 is attributed to 3 hydrogen bonds per water*
 234 *molecule (DDA) (Sun, 2009). The deconvolution of the Raman water bands confirms a*
 235 *reduction in hydrogen bonding in water with the addition of various halogens and their*
 236 *increasing ionic size. Moreover, increasing pressure correlates with an augmented number of*
 237 *hydrogen bonds.*

238

239 4.3. Pressure

240 With increasing pressure, the water stretching band peak at 3428 cm^{-1} undergoes a reduction
241 in intensity and shifts towards the left (e.g., Romanenko et al., 2018), while the smaller peak
242 at 3240 cm^{-1} experiences a slight increase. The observed change stands in contrast to the
243 effects observed during temperature increase (cf., Durickovic et al., 2010) or the addition of
244 halogens (Figure 3). This shift can be interpreted as a transition towards a higher number of
245 hydrogen bonds (from DA to DDAA) in the water molecule network (Sun, 2009, Figure 4). The
246 effect is observable for all three halogens (chlorine, bromine, and iodine) in the saline solutions
247 of this study (Figure 3).

248 Sun (2012) did not observe the pressure effect in their chlorine data and argue against its
249 existence. However, upon normalizing our data in the same way as Sun (2012), the peak at
250 3428 cm^{-1} decreases, and the water bands flatten, yet a clear pressure trend remains
251 (Supplementary Figure S1). It remains unclear why the trend was not observed in Sun (2012).

252 At pressures greater than 1 GPa and ambient temperature, water transforms into ice VI (Figure
253 3). Notably, with increasing halogen concentrations, the water-ice phase transformation shifts
254 to higher pressures. In this study, liquid water/saline solution was observed at 1.1 GPa and
255 0.34 mol/l chlorine, 1.37 GPa and 0.97 mol/l bromine, or 1.27 GPa and 0.67 mol/l iodine. The
256 experimental setup does not precisely determine if the phase boundary shifts to higher
257 pressure or if the liquid state is metastable. Journaux et al. (2013) investigated the impact of
258 NaCl on the phase boundary of ice VI and found the boundary at 1.01 GPa for 1 mol/l, 1.09
259 GPa for 2.5 mol/l, and 1.52 GPa for 4 mol/l at ambient temperature. This boundary shift is
260 much smaller than the observed range, suggesting a metastable liquid phase in our study or
261 other kinetic effects.

262 As a consequence of the pressure-related shape change of the water stretching bands, R_D
263 decreases with increasing pressure for fixed halogen concentrations (Figure 3). Figure 5
264 illustrates the R_D values vs. halogen concentration at different pressures (S_D values in
265 Supplementary Figure S2). Despite some outliers, the values follow a linear trend in the studied
266 range, as previously observed for various temperatures (Durickovic et al., 2010). Within the

267 range of comparable pressures, chlorine exhibits the lowest R_D values, while iodine
268 demonstrates the highest. Comparable trends are also observed for integrated intensities
269 (Supplementary Figure S3) but show larger scatter relative to the R_D trends in Figure 2d and
270 Figure 5.

271

272 4.4. Applications

273 4.4.1. *Natural fluid inclusions with one unknown component (P or X)*

274 R_D can be calculated from Raman spectra of natural fluid inclusions in minerals, as
275 demonstrated by Kawamoto et al. (2013). In their study, saline fluid inclusions in spinel-
276 harzburgite xenoliths collected from the 1991 Pinatubo pumice deposits were examined. The
277 salinity of the fluid inclusions was reported as 5.1 ± 1 wt.% NaCl equivalent (0.87 ± 0.17 mol/l),
278 measured with microthermometry. The authors employed Raman spectroscopy for qualitative
279 water measurements.

280 From the provided Raman spectrum, a R_D value of 0.79 can be calculated. The measured
281 chlorine concentration from microthermometry allows for an estimate of the pressure to be
282 around 0.5 GPa (Figure 5a). This is notably lower than the 2-3 GPa that Kawamoto and
283 colleagues estimated for the formation of the saline fluid inclusions in olivine below the
284 Pinatubo. Given the available information, it can only be speculated whether some (parts) of
285 the olivines formed at a very low pressure of 0.5 GPa, or if the inclusion lost pressure, and it
286 was not fully closed above 0.5 GPa. In this case, the inclusion could at least partially represent
287 the conditions at 0.5 GPa rather than at 2-3 GPa.

288 It is crucial to note that a fluid inclusion that closes between 810 °C and 1050 °C (Kawamoto
289 et al., 2013) will experience a decrease in pressure when cooling down to ambient
290 temperature. This phenomenon is also well observed in HDAC experiments (e.g., Bureau et
291 al., 2010, 2016; Leroy et al., 2019; Louvel et al., 2020a, 2020b) and argues for a higher
292 pressure than the 0.5 GPa that were obtained from the Raman spectrum. However, this sample

293 serves as a good illustration of how pressure can be estimated by Raman in saline fluid
294 inclusions with given salinity.

295

296 4.4.2. *Natural fluid inclusions with two unknown components (P and X)*

297 Difficulties arise when neither pressure nor salinity can be determined with a different method,
298 and only the Raman spectrum is available. This scenario may occur for fluid inclusions that
299 are too small for microthermometry, resulting in a single equation with two unknown
300 parameters that cannot be solved for a distinct value.

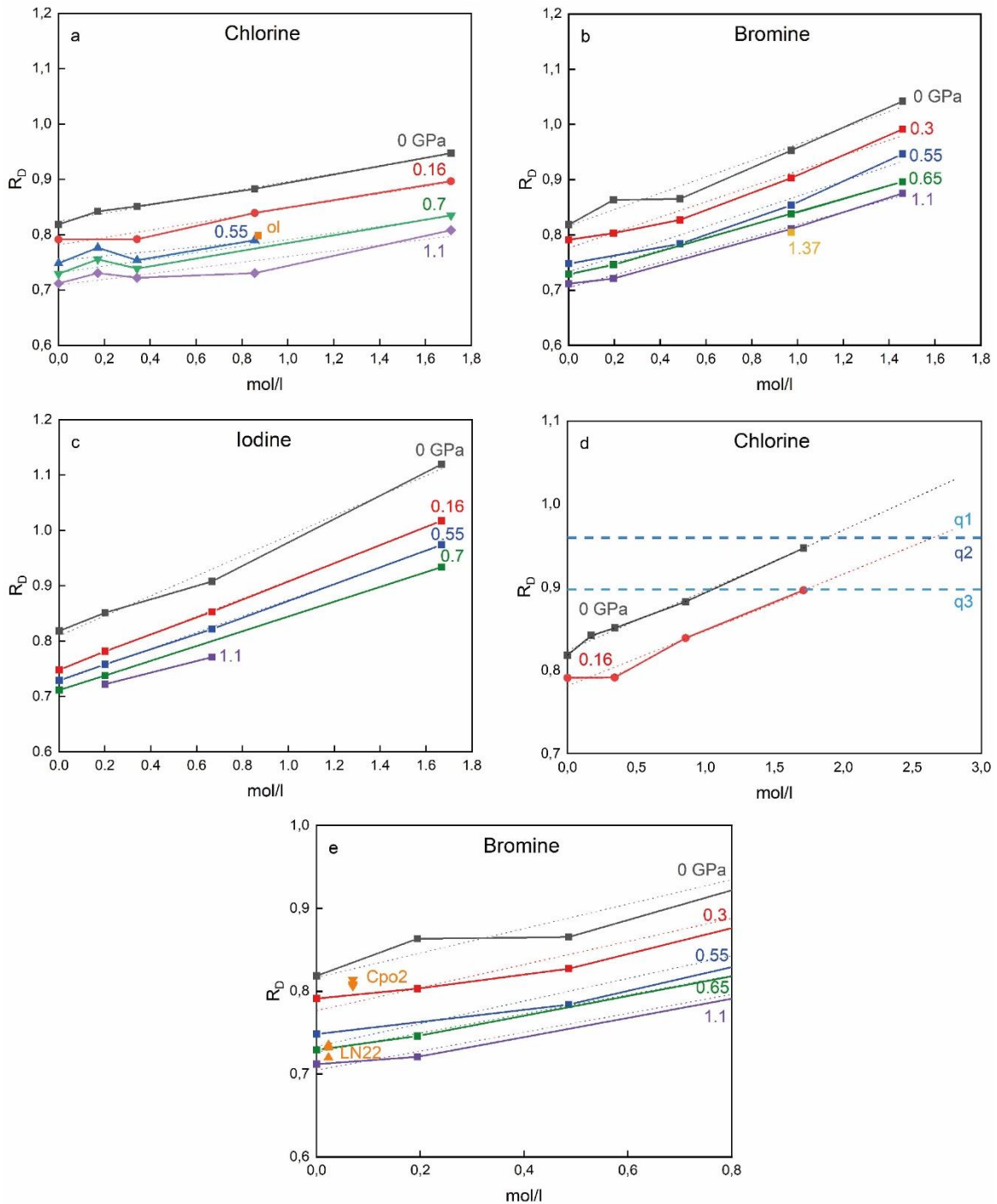
301 Saline fluid inclusions from quartz samples analyzed by Pankrushina et al. (2020) illustrate the
302 pressure dependence in Figure 5d, where R_D values plot as a constant line. For instance, q1
303 has 1.9 mol/L NaCl at ambient pressure and 2.71 mol/L at 0.16 GPa; q2 has 1.88 mol/L and
304 2.69 mol/L; and q3 has 1.02 mol/L and 1.75 mol/L at ambient pressure and at 0.16 GPa,
305 respectively. For an unknown pressure, a single salinity value cannot be determined this way.
306 Particularly at lower salinity concentrations, the range of possible salinities can be drastic: for
307 the three natural samples q1-3, a small pressure increase of 0.16 GPa changes the salinity by
308 42 to 72%. Given the stability field of quartz and saline fluids at room temperature, these are
309 conservative calculations, and a much larger pressure range of > 1 GPa must be considered.

310 However, fluid inclusions can be saturated in NaCl, and halite crystals do coexist with saline
311 fluids in the inclusion (e.g., Brooks et al., 2019). The solubility of NaCl in water at ambient P-T
312 conditions is 317 g/l or 5.4 mol/l (cf. Figure 5). The pressure effect is diminished at NaCl-
313 saturated conditions: Experiments in this study were conducted up to a salinity of 1.71 mol/L
314 for NaCl, but assuming a continuation of the observed linear trend, the difference between 0
315 and 0.16 GPa would be only 16 to 18%.

316 Therefore, the pressure effect in fluid inclusions with high salinity is smaller than in fluid
317 inclusions with low salinity. But as the potential pressure range is large (more than 1 GPa),

318 ignoring the pressure effect can lead to a huge underestimation of the salinity in the fluid, and
 319 Raman spectroscopy alone cannot be used to determine reliable salinities in fluid inclusions.

320



321

322 *Figure 5* R_D values vs halogen concentration for (a) chlorine, (b) bromine, and (c) iodine
 323 are presented in the figure. The colored lines indicate isobars: the solid lines connect the data
 324 points, while the dotted lines represent trend lines. Like the Raman water bands and the R_D

325 values, the isobars exhibit the steepest slope for high concentrations of iodine and become
326 flatter with smaller ionic halogen size, but also with increasing pressure. (a) "ol" data are from
327 a natural fluid inclusion in olivine (Kawamoto et al., 2013). (d) Calculated R_D values for natural
328 fluid inclusions in quartz demonstrate the pressure effect: q1 has 1.9 mol/L NaCl equivalent at
329 ambient pressure and 2.71 mol/L at 0.16 GPa; q2 has 1.88 mol/L and 2.69 mol/L; and q3 has
330 1.02 mol/L and 1.75 mol/L at ambient pressure and at 0.16 GPa, respectively. The fluid
331 inclusions were analyzed by Pankrushina et al. (2020) (sample names are q1 = 672; q2 =
332 33604; q3 = 20512). (e) Cpo2 and LN22 are experimental HDAC samples. Bromine content
333 was analyzed with X-ray fluorescence following the methods reported in Bureau et al. (2010)
334 and Grützner et al. (2024).

335

336 4.4.3. Heavy halogens in HDAC experiments

337 The heavy halogens bromine and iodine typically play a minor role in natural fluid inclusions.
338 The Cl/Br ratio in seawater is approximately 30, and the Cl/I ratio is around 50 (cf. Shaw and
339 Cooper, 1957 for iodine). Due to enrichment and depletion processes in the Earth's mantle,
340 Cl/Br ratios can vary significantly, ranging, for example, in diamond inclusions from 1 to 500
341 (Jonson et al., 2000). Despite their low concentration and minor role in fluid inclusions, heavy
342 halogens are highly reactive and serve as important chemical agents in Earth's atmosphere
343 (Fehn et al., 2012). Particularly for bromine, volcanoes have been recognized as significant
344 contributors (Gerlach et al., 2004), if not the primary controlling factor (Pyle and Mather, 2009),
345 to the current atmospheric content. This recognition is crucial, as bromine can be
346 approximately 60 times more efficient (Sinnhuber et al., 2009) than chlorine in the destruction
347 of stratospheric ozone (Daniel et al., 1999; Gerlach et al., 2004).

348 Over the past few decades, numerous studies have conducted high-pressure experiments on
349 bromine- and iodine-bearing fluids interacting with silica melts in hydrothermal diamond anvil
350 cells (HDAC). In these studies, the halogen content in the fluid was measured using
351 synchrotron X-ray fluorescence (Bureau et al., 2010, 2016; Kawamoto et al., 2014; Leroy et

352 al., 2019; Louvel et al., 2020a, 2020b). These experiments provide valuable insights into the
353 behavior of heavy halogens during fluid-magma degassing processes.

354 However, these experiments entail complex setups and lack reliable and easily adaptable
355 pressure sensors. The fluorescence wavelength shift of ruby is a commonly used pressure
356 sensor (e.g., Chervin et al., 2001; Shen et al., 2020), but it cannot be applied in experiments
357 conducted at elevated temperatures where ruby spheres dissolve. Other pressure indicators,
358 like X-ray diffraction of gold particles, are only reliable at higher temperatures (cf. Grützner et
359 al., 2024; Louvel et al., 2020b). Pressure monitoring in these HDAC experiments is essential
360 to understand the pressure effect on halogen partitioning between silicate melts and aqueous
361 fluids. Moreover, it is crucial to exclude pressure loss processes during the experiment (cf.
362 Bureau et al., 2010, 2016; Leroy et al., 2019; Louvel et al., 2020a, 2020b).

363 Most HDAC experiments are conducted at high temperatures, reaching several hundred
364 degrees Celsius (e.g., Bureau et al., 2010, 2016; Grützner et al., 2024; Leroy et al., 2019;
365 Louvel et al., 2020a, 2020b). The elevated temperature introduces an additional variable to the
366 shift change of the water bands, as they also change with varying temperature (Krishnamurthy
367 et al., 1983; Ratcliffe and Irish, 1982).

368 Thus far, residual pressure can be monitored at ambient temperature, for example, before and
369 after the experiment, once the fluid has been cooled down to room temperature. Figure 5e
370 illustrates two samples used for test measurements, following the experimental setup and the
371 analytical methods for bromine concentration reported in Grützner et al. (2024). These
372 samples represent experiments that tested the degassing reaction of a bromine-doped basalt
373 melt into an aqueous fluid. Experiments were conducted at high temperatures (above the
374 basalt solidus) and pressures of up to 1.7 GPa in a hydrothermal diamond anvil cell (cf.
375 Grützner et al., 2024, for a detailed description of the experiments). Bromine concentrations of
376 0.07 mol/L for sample LN22 and 0.023 mol/L for Cpo2 were measured in the fluid by
377 synchrotron x-ray fluorescence (SXRF) during the experiments. Raman spectra of the aqueous
378 fluids were analyzed after the experiment under room temperature conditions. Bromine

379 concentrations from SXRF, together with the Raman spectra, allow estimating pressure ranges
380 of 0.7 to 0.9 GPa for LN22 and 0.1 to 0.2 GPa for Cpo2. These promising results show that
381 Raman water bands can be used as pressure or salinity indicators from room to high
382 temperatures, providing additional pressure-concentration-related temperature calibrations
383 are performed.

384

385 5. Conclusion

386 Our new experimental dataset demonstrates that the impact of halogens on the change of
387 Raman water band shifts increases with ionic size from chlorine over bromine to iodine. To
388 address and compare these changes, we calculated the numerical value R_D . Our experiments
389 further show that increased pressure diminishes the impact of the halogen shift change to a
390 different extent for each of the three halogens. This can have drastic consequences for the
391 salinity calculation of fluid inclusions in minerals like quartz or olivine. Especially in the range
392 of low salinity, the concentration can be strongly underestimated if the pressure effect is
393 ignored. Either pressure or salinity needs to be determined by an independent method. For
394 experiments performed in diamond anvil cells with halogens in aqueous fluids, the change of
395 Raman water band shifts can be a beneficial (with some restrictions) tool to monitor the
396 pressure at room temperature, if salinity is known, and inversely this change can be used to
397 monitor the salinity.

398

399 6. Acknowledgments

400 This project was funded by the ANR Projet de Recherche Collaborative VOLC-HAL-CLIM
401 (Volcanic Halogens: from Deep Earth to Atmospheric Impacts), ANR-18-CE01-0018 (Hélène
402 Bureau). Tobias Grützner is grateful for the EU Marie Skłodowska-Curie Fellowship “ExCliso”
403 (Project ID 101017762). We thank K. Béneut for his support with the Raman laser we used
404 for our experiments at the IMPMC and Y. Guarnelli for his help with the DAC alignment. We

405 are very grateful to E.A. Pankrushina for providing the raw dataset of Raman spectra from
406 her study. We thank the two reviewers for their helpful comments to improve the manuscript
407 and editor Claudia Romano is thanked for handling the manuscript.

408

409

410 Statement: During the preparation of this work the authors used ChatGPT 3.5 to correct
411 errors of spelling, punctuation, grammar and to improve the syntax in several chapters of the
412 manuscript. After using this tool, the authors reviewed and edited the content and take full
413 responsibility for the content of the publication.

414

415 7. References

- 416 Aiuppa, A., Baker, D.R., & Webster, J.D., 2009. Halogens in volcanic systems. *Chem. Geol.*,
417 **263(1-4)**, 1-18. <https://doi.org/10.1016/j.chemgeo.2008.10.005>.
- 418 Bakker, R.J., 2004. Raman spectra of fluid and crystal mixtures in the systems H₂O, H₂O-NaCl
419 and H₂O-MgCl₂ at low temperatures: applications to fluid-inclusion research. *Can. Mineral.*
420 **42**, 1283-1314. <https://doi.org/10.2113/gscanmin.42.5.1283>.
- 421 Besemer, M., Bloemenkamp, R., Ariese, F., van Manen, H.-J., 2016. Identification of multiple
422 water-iodide species in concentrated NaI solutions based on the raman bending vibration of
423 water. *J. Phys. Chem. A* **120(5)**, 709-714. <https://doi.org/10.1021/acs.jpca.5b10102>.
- 424 Brooks, H.L., Dragovic, B., Lamadrid, H.M., Caddick, M.J., Bodnar, R.J., 2019. Fluid capture
425 during exhumation of subducted lithologies: A fluid inclusion study from Sifnos, Greece.
426 *Lithos* **332-333**, 120-134. <https://doi.org/10.1016/j.lithos.2019.01.014>.
- 427 Bureau, H., Keppler, H., and Métrich, N., 2000. Volcanic degassing of bromine and iodine:
428 Experimental fluid/melt partitioning data and applications to stratospheric chemistry: *Earth*
429 *Planet. Sci. Lett.* **183**, 51-60. [https://doi.org/10.1016/S0012-821X\(00\)00258-2](https://doi.org/10.1016/S0012-821X(00)00258-2).
- 430 Bureau, H., Foy, E., Raepsaet, C., Somogyi, A., Munsch, P., Simon, G., Kubsy, S., 2010.
431 Bromine cycle in subduction zones through in situ Br monitoring in diamond anvil cells.
432 *Geochim. Cosmochim. Acta* **74**, 3839–3850. <https://doi.org/10.1016/j.gca.2010.04.001>.
- 433 Bureau, H., Auzende, A.-L., Marocchi, M., Raepsaet, C., Munsch, P., Testemale, D., Mézouar,
434 M., Kubsy, S., Carrière, M., Ricolleau, A., Fiquet, G., 2016. Modern and past volcanic
435 degassing of Iodine. *Geochim. Cosmochim. Acta* **173**, 114–125.
436 <https://doi.org/10.1016/j.gca.2015.10.017>.
- 437 Chervin, J.C, Canny B., Besson, J. M., Pruzan, P., 1995. A diamond anvil cell for IR
438 microspectroscopy. *Rev. Sci. Instrum.* **66** (3), 2595-2598. <https://doi.org/10.1063/1.1145594>.

439 Chervin J.C., Canny B., Mancinelli M., 2001. Ruby-spheres as pressure gauge for optically
440 transparent high pressure cells. *High Press. Res.* **21**, 305–314.
441 <https://doi.org/10.1080/08957950108202589>.

442 Daniel, J.S., Solomon, S., Portmann, R.W., 1999. Stratospheric ozone destruction: The
443 importance of bromine relative to chlorine. *J. Geophys. Res.* **104**, 23871-23880.
444 <https://doi.org/10.1029/1999JD900381>.

445 Dubessy J., Lhomme, T., Boiron, M-C., Rull, F., 2002. Determination of Chlorinity in Aqueous
446 Fluids Using Raman Spectroscopy of the Stretching Band of Water at Room Temperature:
447 Application to Fluid Inclusions. *Appl. Spectrosc.* **56(1)**, 99-106.

448 Đuričković, I., Marchetti, M., Claverie, R., Bourson, P., Chassot, J-M., Fontana, M.D., 2010.
449 Experimental study of NaCl aqueous solutions by Raman spectroscopy: Towards a new
450 optical sensor. *Appl. Spectrosc.* **64(8)**, 853-857.
451 <https://doi.org/10.1366/000370210792080984>.

452 Fehn, U., 2012. Tracing crustal fluids: Applications of natural ¹²⁹I and ³⁶Cl. *Annu. Rev. Earth
453 Planet. Sci.* **40**, 45-67. <https://doi.org/10.1146/annurev-earth-042711-105528>.

454 Georgiev, G.M., Kalkanjiev, T.K., Petrov, V.P., Nickolov, Zh., 1984. Determination of Salts in
455 Water Solutions by a Skewing Parameter of the Water Raman Band. *Appl. Spectrosc.* **38(4)**,
456 593-595. <https://doi.org/10.1366/0003702844555106>.

457 Gerlach, T.M., 2004. Volcanic source of tropospheric ozone-depleting trace gases. *Geochem.
458 Geophys. Geosyst.* **5**, Q09007. <https://doi.org/10.1029/2004GC000747>.

459 Grützner, T., Bureau, H., Boulard, E., Munsch, P., Guignot, N., Siebert, J., Guarnelli, Y., 2024.
460 An in-situ experimental HP/HT study on bromine release from a natural basalt. *Chem. Geol.*
461 **644**, 121869. <https://doi.org/10.1016/j.chemgeo.2023.121869>.

462 Johnson, L.H., Burgess, R., Turner, G., Milledge, H.J., Harris, J.W. 2000. Noble gas and
463 halogen geochemistry of mantle fluids: comparison of African and Canadian diamonds.
464 *Geochim. Cosmochim. Acta* **64**, 717-732. [https://doi.org/10.1016/S0016-7037\(99\)00336-1](https://doi.org/10.1016/S0016-7037(99)00336-1).

465 Journaux, B., Daniel, I., Caracas, R., Montagnac, G., Cardon, H., 2013. Influence of NaCl on
466 ice VI and ice VII melting curves up to 6 GPa, implications for large icy moons. *Icarus* **226**,
467 355-363. <https://doi.org/10.1016/j.icarus.2013.05.039>.

468 Kawamoto, T., Yoshikawa, M., Kumagai, Y., Mirabueno, M.H.T., Okuno, M., Kobayashi, T.,
469 2013. Mantle wedge infiltrated with saline fluids from dehydration and decarbonation of
470 subducting slab. *Proc. Nat. Acad. Sci. USA.*, **110(24)**, 9663-9668.
471 <https://doi.org/10.1073/pnas.1302040110>.

472 Kawamoto, T., Mibe, K., Bureau, H., Reguer, S., Mocuta, C., Kubsy, S., Thiaudière, D., Ono,
473 S., Kogiso, T., 2014. Large-ion lithophile elements delivered by saline fluids to the sub-arc
474 mantle. *Earth Planets Space* **66**, 61. <https://doi.org/10.1186/1880-5981-66-61>.

475 Krishnamurthy, S., Bansil, R., Wiafe-Akente, J., 1983. Low-frequency Raman spectrum of
476 supercooled water. *J. Chem. Phys.* **79**, 5863-5870. <https://doi.org/10.1063/1.445756>.

477 Leroy, C.; Bureau, H., Sanloup, C., Raepsaet, C., Glazirin, K., Munsch, P., Harmand, M.,
478 Prouteau, G., Khodja, H., 2019. Xenon and iodine behaviour in magmas. *Earth. Planet. Sci.*
479 *Lett.* **522**, 144-154. <https://doi.org/10.1016/j.epsl.2019.06.031>.

480 Louvel, M., Cadoux, A., Brooker, R.A., Proux, O., Hazemann, J-L., 2020a. New insights on Br
481 speciation in volcanic glasses and structural controls on halogen degassing. *Am. Min.* **105**,
482 795-802. <https://doi.org/10.2138/am-2020-7273>.

483 Louvel, M., Sanchez-Valle, C., Malfait, W.J., Pokrovski, G.S., Borca, C.N., Grolimund, D.,
484 2020b. Bromine speciation and partitioning in slab-derived aqueous fluids and silicate melts
485 and implications for halogen transfer in subduction zones. *Solid Earth* **11**, 1145-1161.
486 <https://doi.org/10.5194/se-11-1145-2020>.

487 Mernagh, T.P., Wilde, A.R., 1989. The use of the laser Raman microprobe for the
488 determination of salinity in fluid inclusions. *Geochim. Cosmochim. Acta* **53(4)**, 765-771.
489 [https://doi.org/10.1016/0016-7037\(89\)90022-7](https://doi.org/10.1016/0016-7037(89)90022-7).

490 Moncada, D., Bodnar, R.J., 2012. Raman spectroscopy technique to determine the salinity of
491 fluid inclusions, PACROFI-XI (Pan-American Current Research on Fluid Inclusions)
492 Conference, pp. 67.

493 Ni, P., Ding, J., Rao, B., 2006. In situ cryogenic Raman spectroscopic studies on the synthetic
494 fluid inclusions in the systems H₂O and NaCl-H₂O. *Chin. Sci. Bull.* **51(1)**, 108-114.
495 <https://doi.org/10.1007/s11434-004-0256-5>.

496 Pankrushina, E.A., Krupenin, M.T., Shchapova, Y.V., Kobuzov, A.S., Garaeva, A.A., Votyakov,
497 S.L., 2020. The study of fluid inclusion salinity in minerals by raman spectroscopy revisited.
498 In: Votykov, S., Kiseleva, D., Grokhovsky, V., Shchapova, J. (eds.), *Minerals: Structure,*
499 *Properties, Methods of Investigation: Proceedings of the 10th All-Russian Youth Scientific*
500 *Conference* (pp. 175-183). Springer International Publishing. <https://doi.org/10.1007/978-3->
501 [030-49468-1_23](https://doi.org/10.1007/978-3-030-49468-1_23).

502 Pyle, D.M., Mather, T.A., 2009. Halogens in igneous processes and their fluxes to the
503 atmosphere and oceans from volcanic activity: A review. *Chem. Geol.* **263**, 110-121.
504 <https://doi.org/10.1016/j.chemgeo.2008.11.013>.

505 Ratcliffe, C.I., Irish, D.E., 1982. Vibrational spectral studies at elevated temperatures and
506 pressures. Raman studies of liquid water up to 300 °C. *J. Phys. Chem.* **86**, 4897-4905.
507 <https://doi.org/10.1021/j100222a013>.

508 Romanenko, A.V., Rashchenko S.V., Goryainov, S.V., Likhacheva
509 <https://doi.org/10.1177/0003702817752487>, A.Y., Korsakov, A.V., 2018. In Situ Raman
510 Study of Liquid Water at High Pressure. *Appl. Spectrosc.* **72(6)**, 847-852.
511 <https://doi.org/10.1177/0003702817752487>.

512 Shaw, T., Cooper, L., 1957. State of Iodine in Sea Water. *Nature* **180**, 250.
513 <https://doi.org/10.1038/180250a0>.

514 Shen, G., Wang, Y., Dewaele, A., Wu, C., Fratanduono, D.E., Eggert, J., Klotz, S., Dziubek,
515 K.F., Loubeyre, P., Fat'yanov, O.V., Asimov, P.D., Mashimo, T., Wentzcovitch, R.M.M., 2020.

516 Toward an international practical pressure scale: A proposal for an IPPS ruby gauge (IPPS-
517 Ruby2020). *High Press. Res.* **40(3)**, 299-314.
518 <https://doi.org/10.1080/08957959.2020.1791107>.

519 Sinnhuber, B.-M., Sheode, N., Sinnhuber, M., Chipperfield, M.P., Feng, W., 2009. The
520 contribution of anthropogenic bromine emissions to past stratospheric ozone trends: A
521 modelling study, *Atmos. Chem. Phys.*, **9(8)**, 2863-2871. [https://doi.org/10.5194/acp-9-2863-](https://doi.org/10.5194/acp-9-2863-2009)
522 2009.

523 Sun, Q., 2009. The Raman OH stretching bands of liquid water. *Vib. Spectrosc.* **51**, 213-217.
524 <https://doi.org/10.1016/j.vibspec.2009.05.002>.

525 Sun, Q., 2012. Raman spectroscopic study of the effects of dissolved NaCl on water structure.
526 *Vib. Spectrosc.* **62**, 110-114. <https://doi.org/10.1016/j.vibspec.2012.05.007>.

527 Sun, Q., Zhao, L., Li, N., Liu, J., 2010. Raman spectroscopic study for the determination of Cl-
528 concentration (molarity scale) in aqueous solutions: Application to fluid inclusions. *Chem.*
529 *Geol.* **272(1-4)**, 55-61. <https://doi.org/10.1016/j.chemgeo.2010.02.004>.

530 Terpstra, P., Combes, D., Zwick, A., 1990. Effect of salts on dynamics of water: A Raman
531 spectroscopy study. *J. Chem. Phys.* **92**, 65-70. <https://doi.org/10.1063/1.458418>.

532 Walrafen, G.E., Fisher, M.R., Hokmabadi, M.S., Yang, W.-H., 1986. Temperature dependence
533 of the low- and high-frequency Raman scattering from liquid water. *J. Chem. Phys.* **85(12)**,
534 6970-6982. <https://doi.org/10.1063/1.451384>.

535

536

537

8. Tables

	NaCl				max(NaCl) ^a
g/l	10	20	50	100	317
mol/l	0.17	0.34	0.86	1.71	5.42
wt.%	0.99	1.96	4.76	9.09	24.07

	NaBr				max(NaBr) ^a
g/l	20	50	100	150	905
mol/l	0.19	0.49	0.97	1.46	8.80
wt.%	1.96	4.76	9.09	13.04	47.51

	NaI			max(NaI) ^a
g/l	30	100	250	1793
mol/l	0.20	0.67	1.67	11.96
wt.%	2.91	9.09	20.00	64.20

^a maximum solubility in H₂O at 20 °C and ambient pressure.

538

539 *Table 1 Salt concentration in the starting solutions and maximum solubility values.*

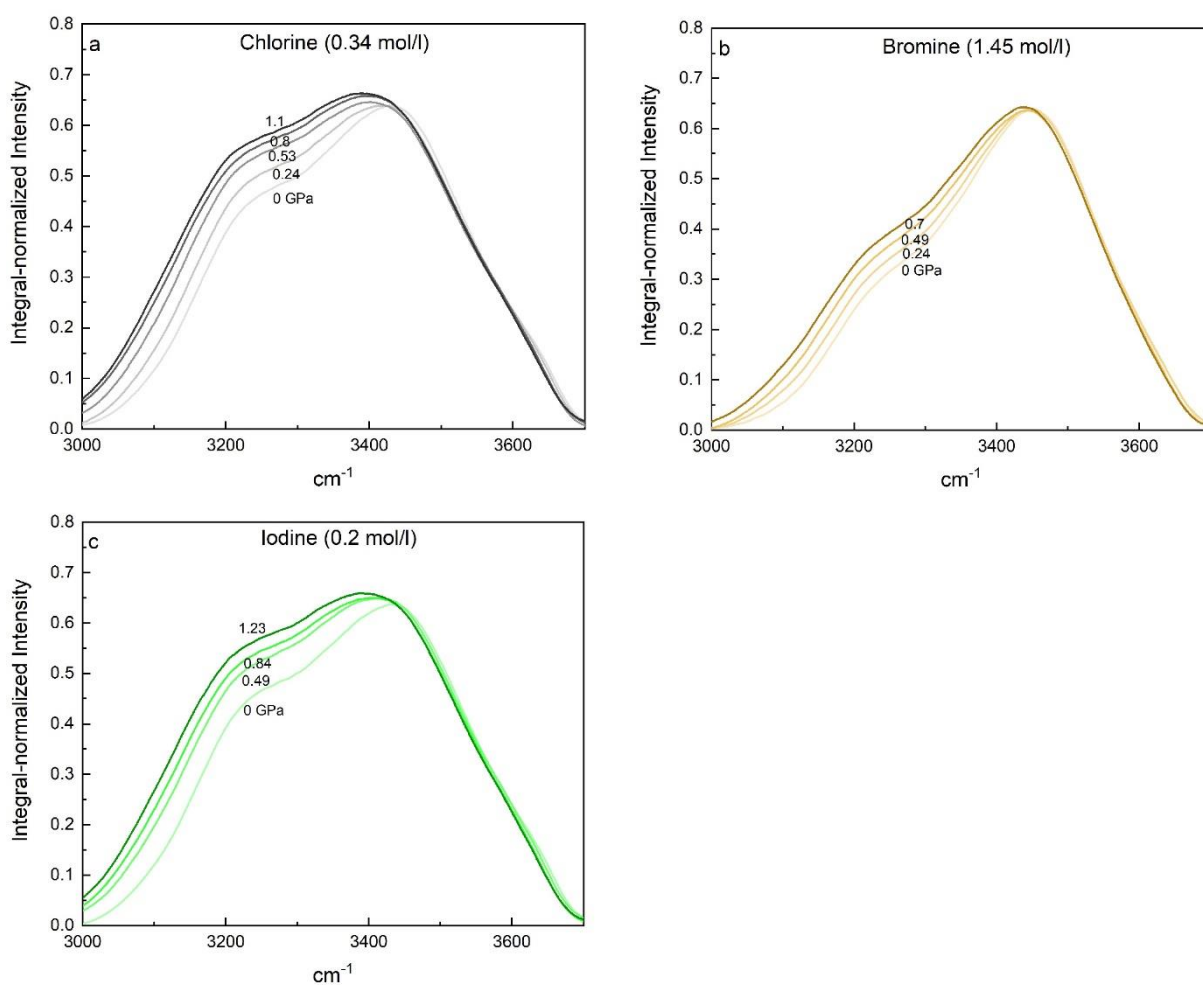
540

541

542 9. Supplementary material

543 Supplementary Tables with Raman raw data are stored under
544 <https://data.mendeley.com/datasets/tnckfpjcv/1>.

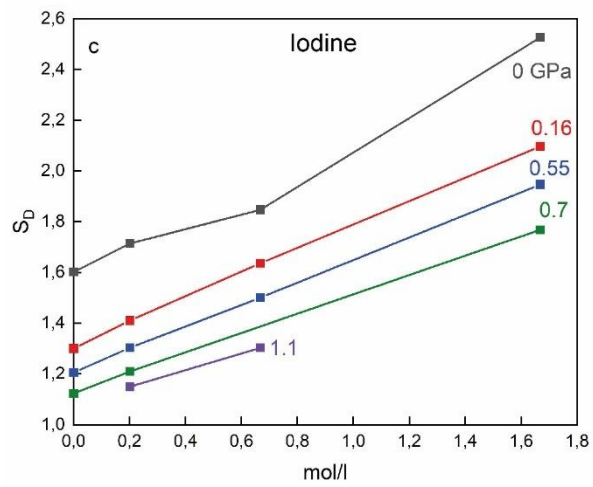
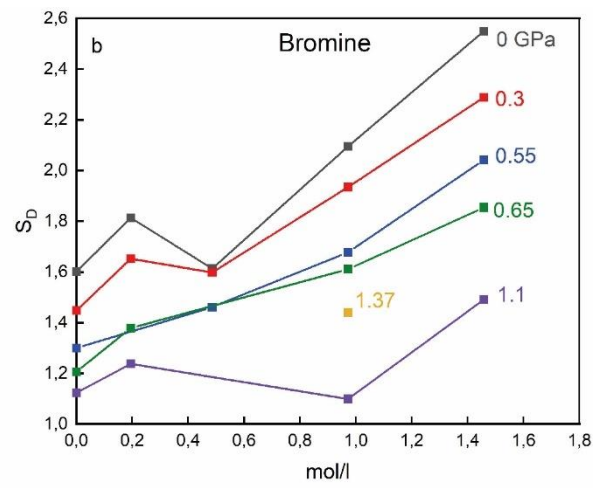
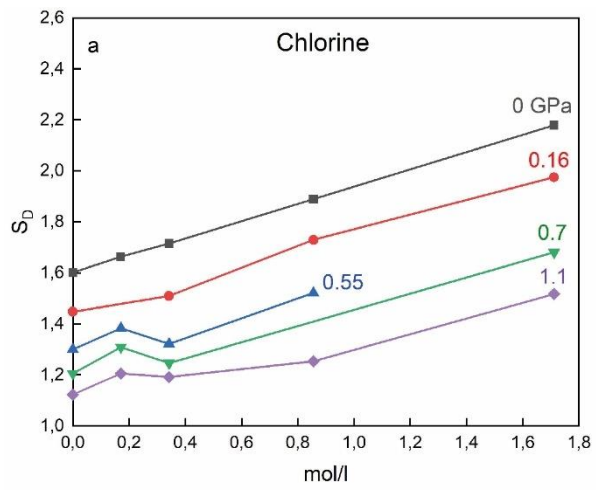
545



546

547 *Figure S1 The Raman water bands of saline solutions are presented with fixed halogen*
548 *concentrations and varying pressure: a) 0.34 mol/l chlorine, b) 1.45 mol/l bromine, and c) 0.2*
549 *mol/l iodine. The pressure is indicated in GPa on the spectra. Notably, the intensities are*
550 *normalized to their integrated intensities for the presented range of 3000 to 3600 cm^{-1} . The*
551 *resulting peaks exhibit a smaller reduction than the spectra in Figure 3 but a leftward shift in*
552 *the spectra indicates a clear pressure effect.*

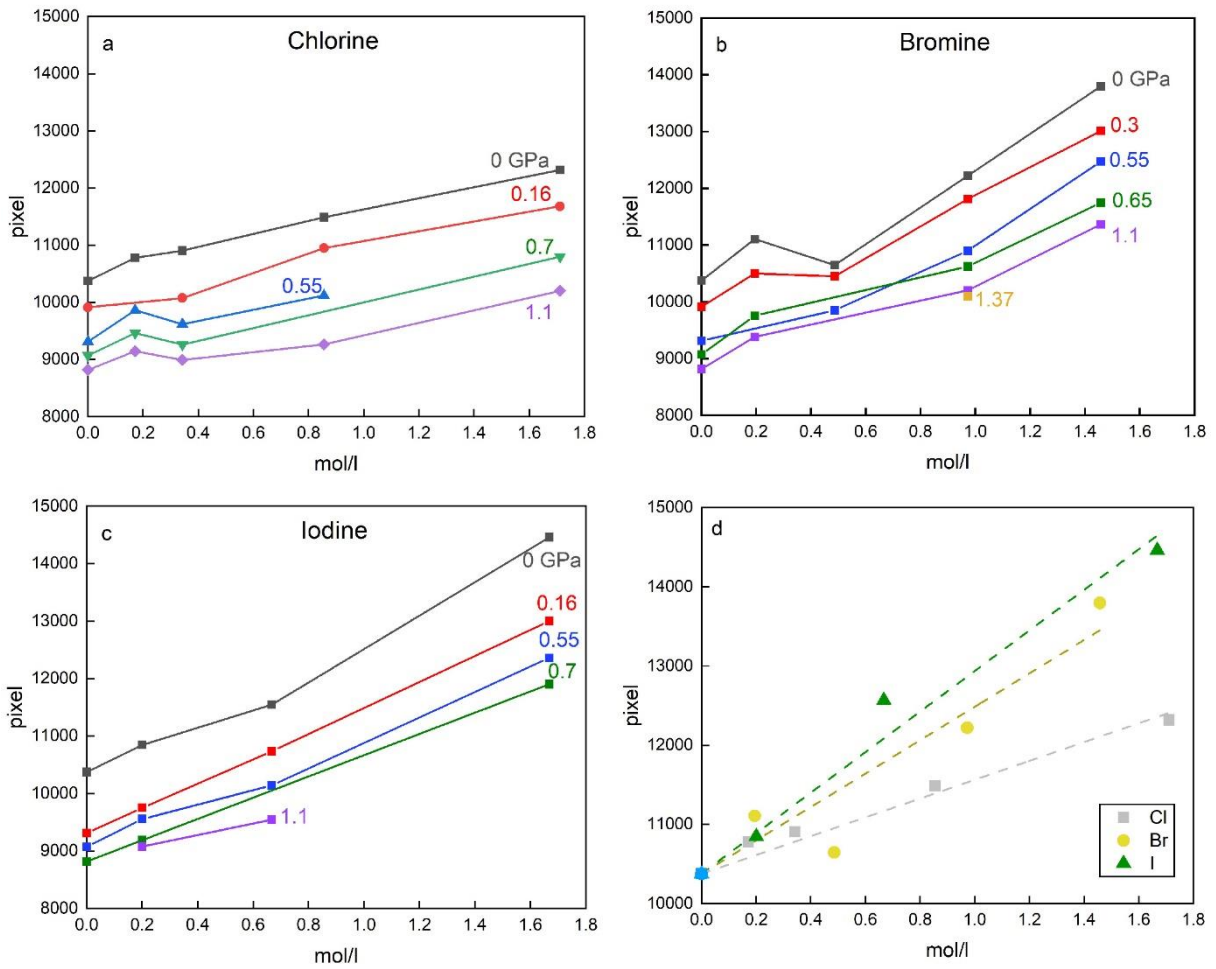
553



554

555 *Figure S2* S_D values vs halogen concentration for a) chlorine, b) bromine, and c) iodine
 556 calculated after Durickovic et al. (2010).

557

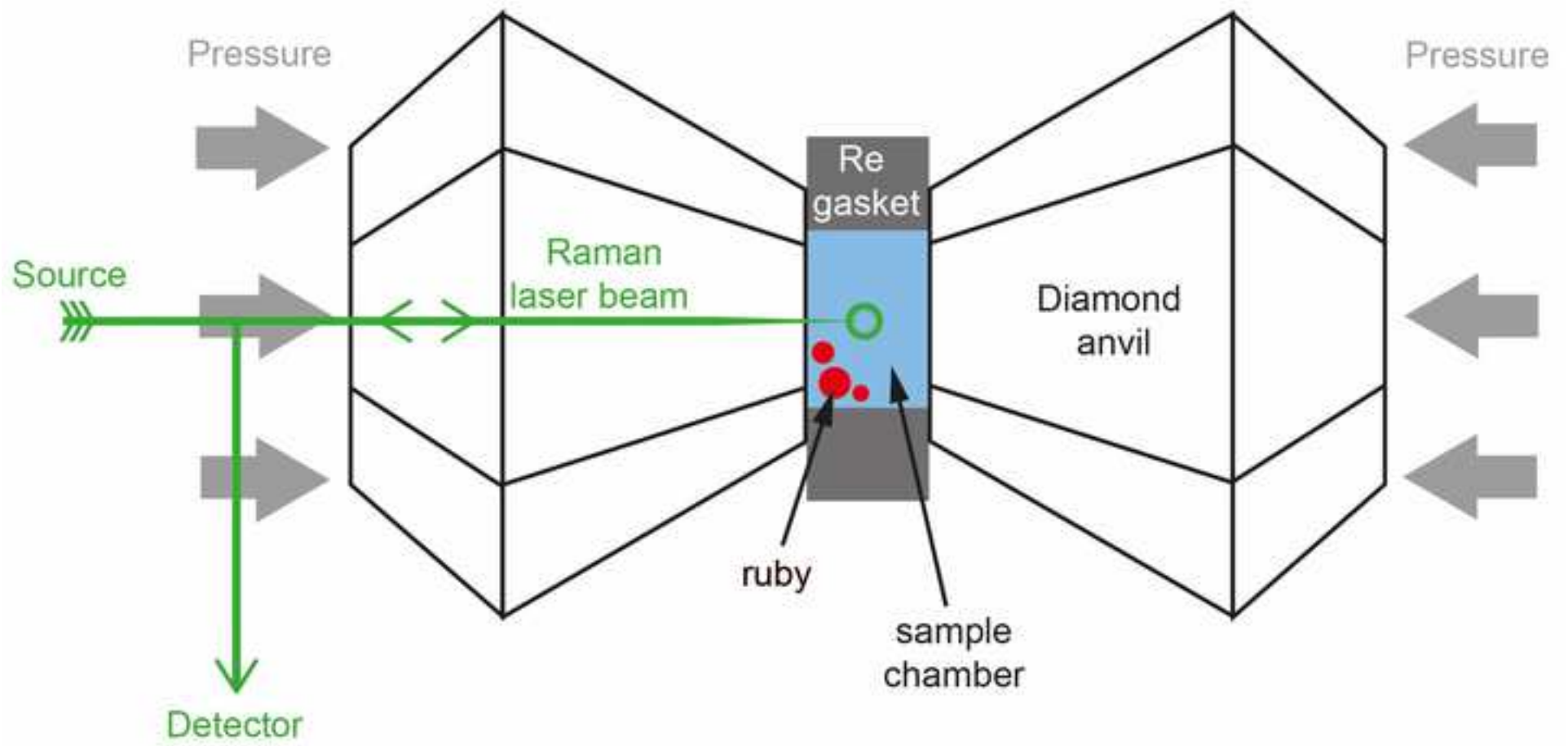


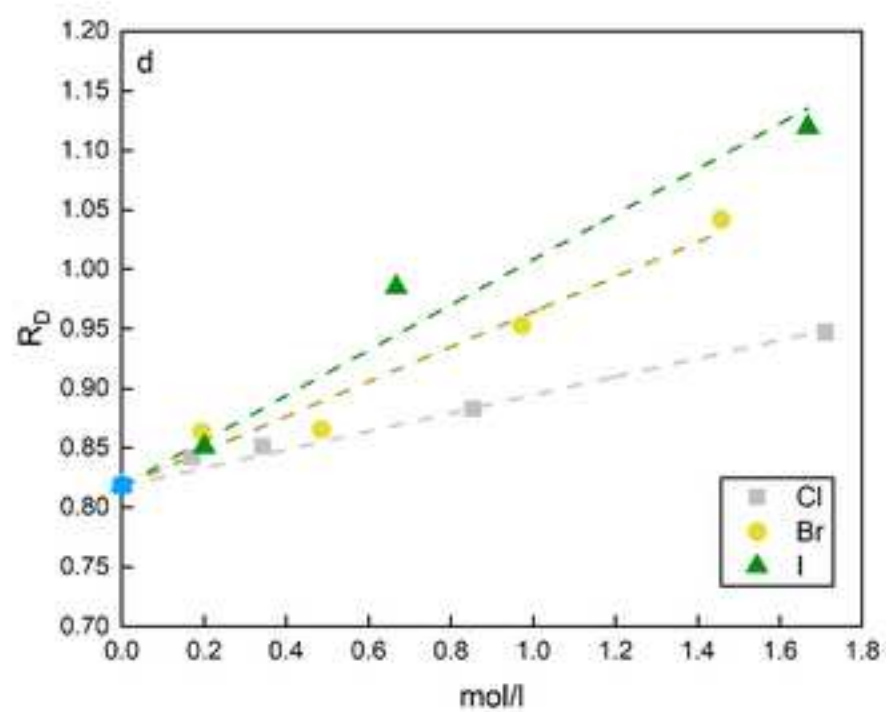
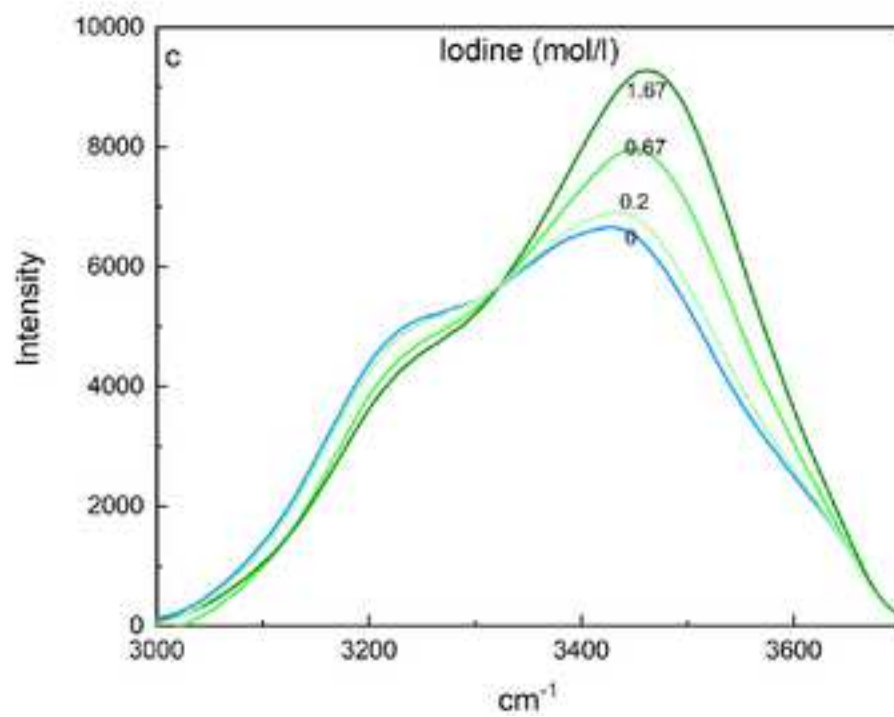
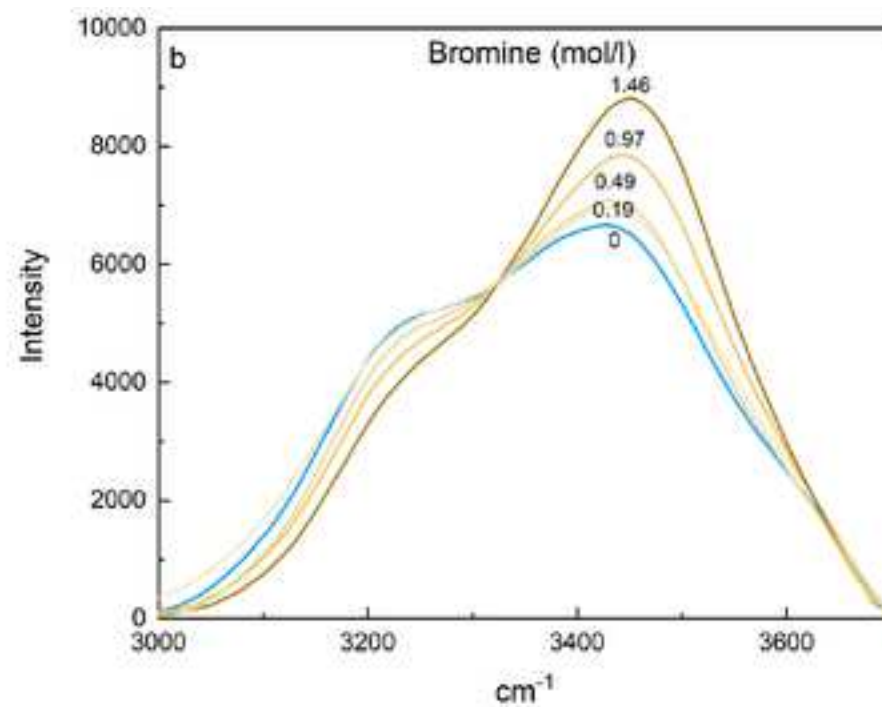
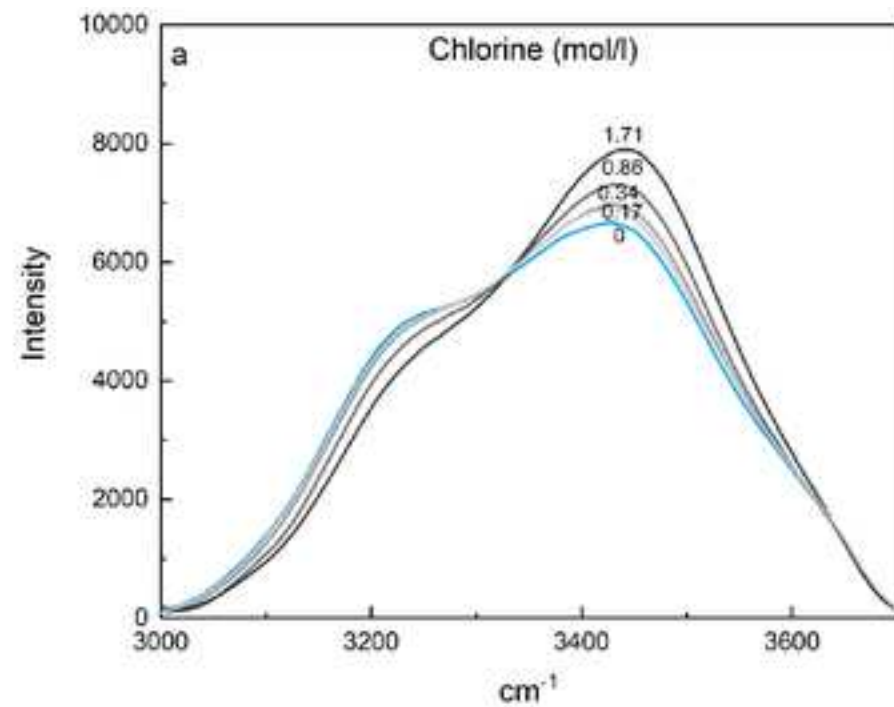
558

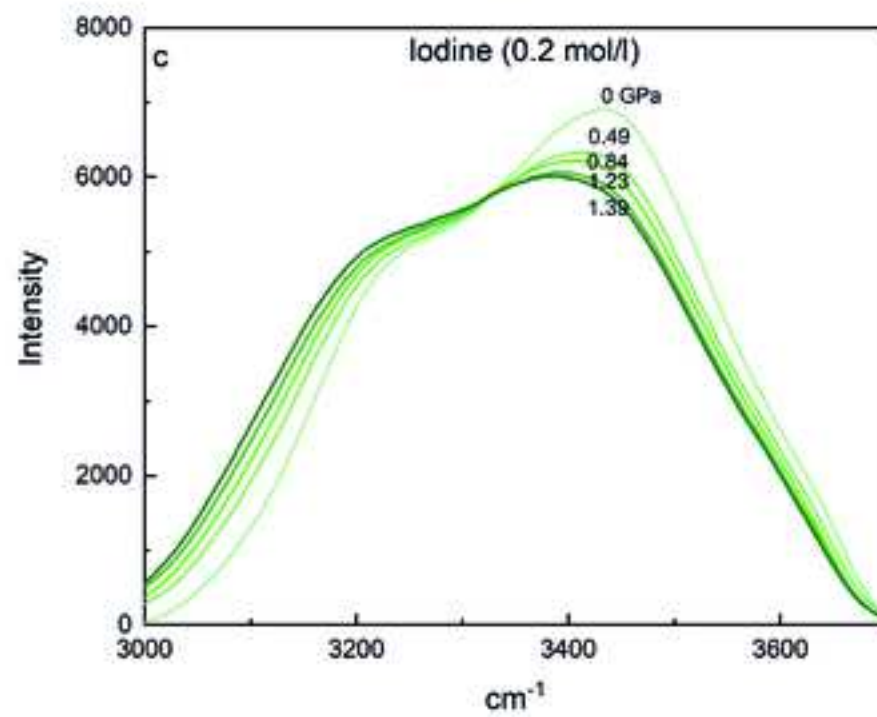
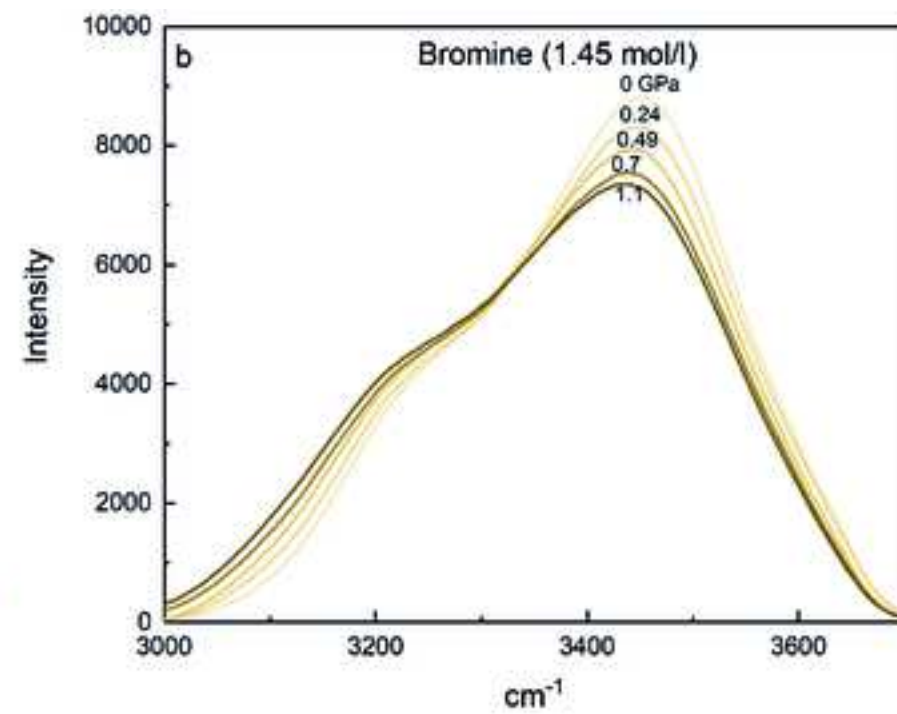
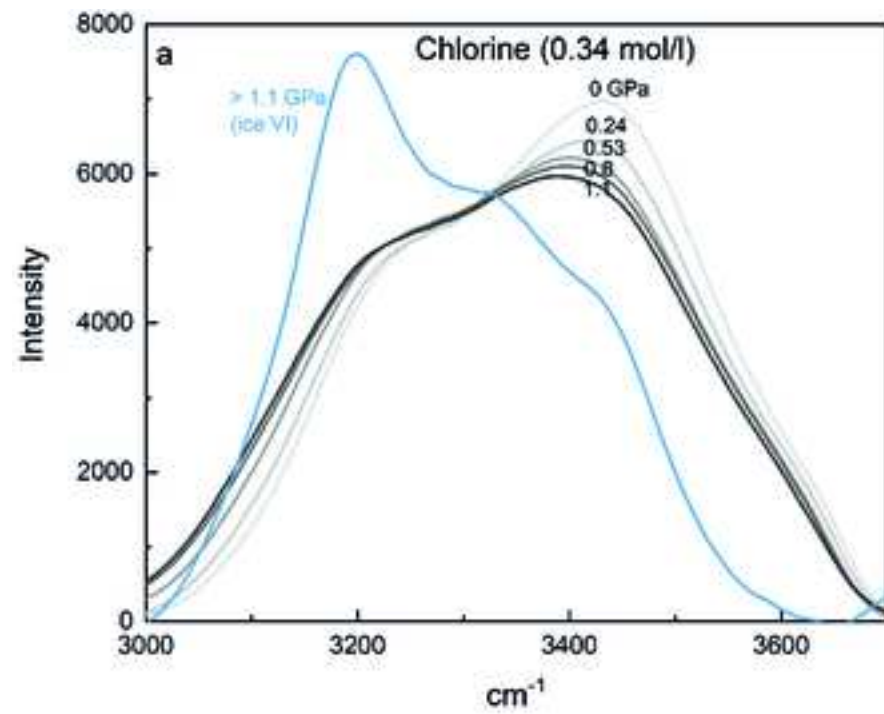
559 *Figure S3 Integrated intensities vs halogen concentration for (a) chlorine, (b) bromine, (c)*
 560 *iodine, and (d) all three elements at ambient pressure show comparable trends but large*
 561 *scatter relative to the R_D values. The intensities were integrated over the range of 3000 to 3600*
 562 *cm^{-1} .*

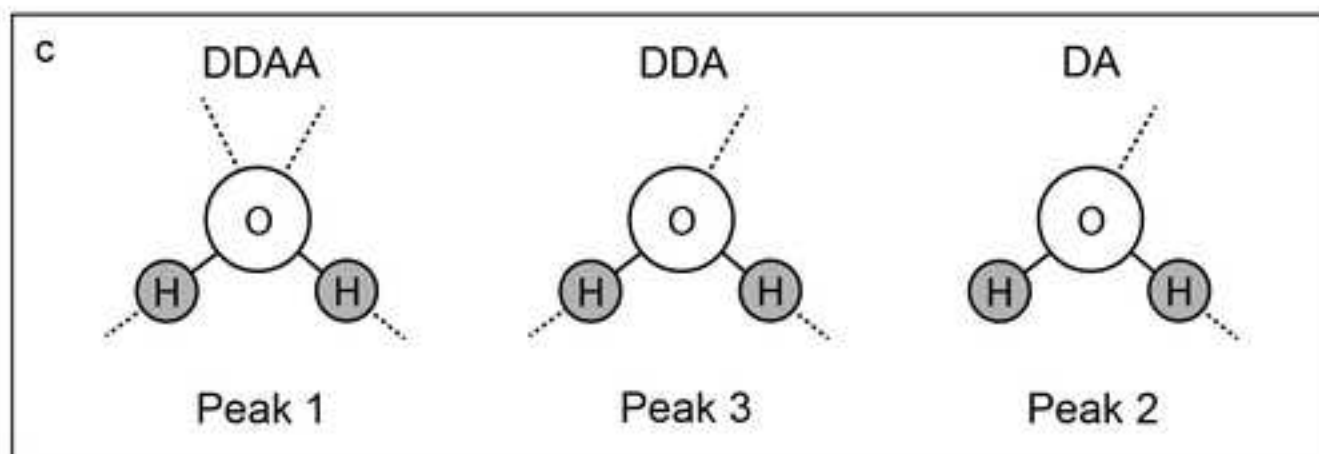
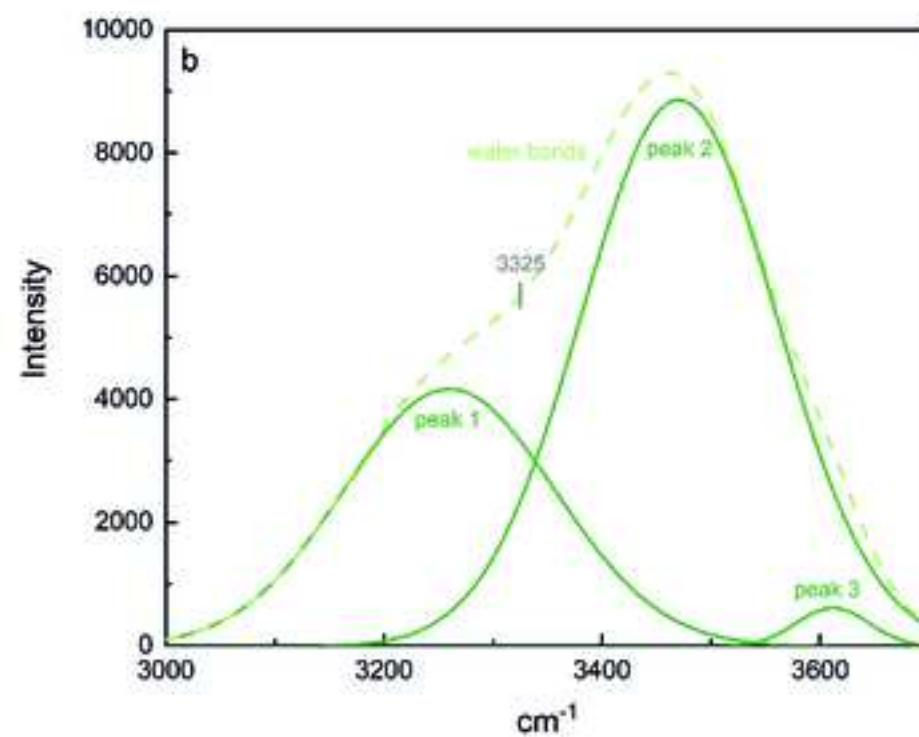
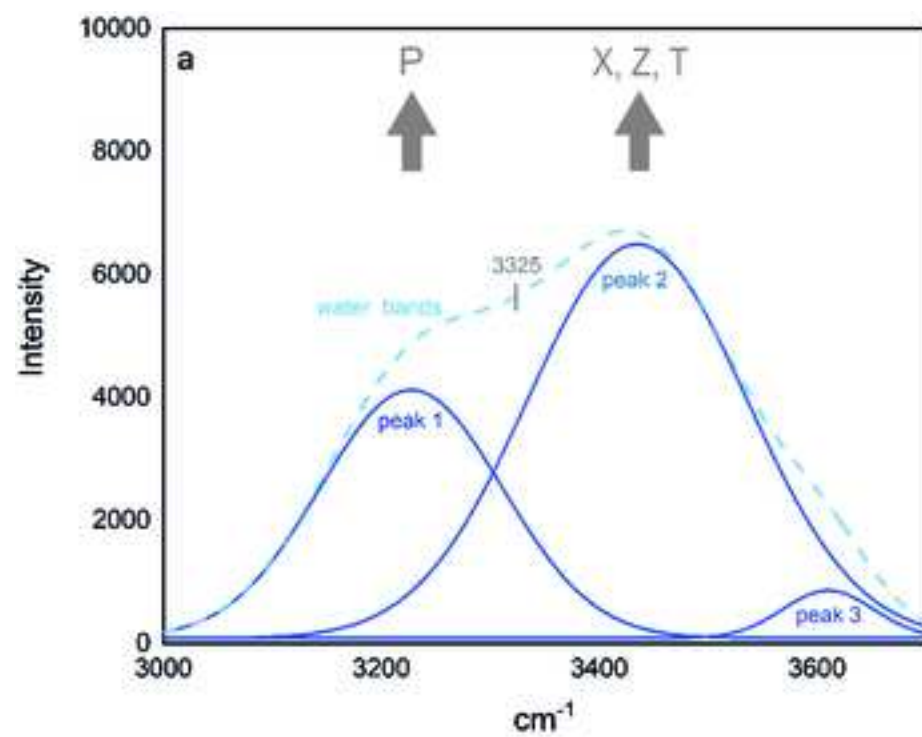
563

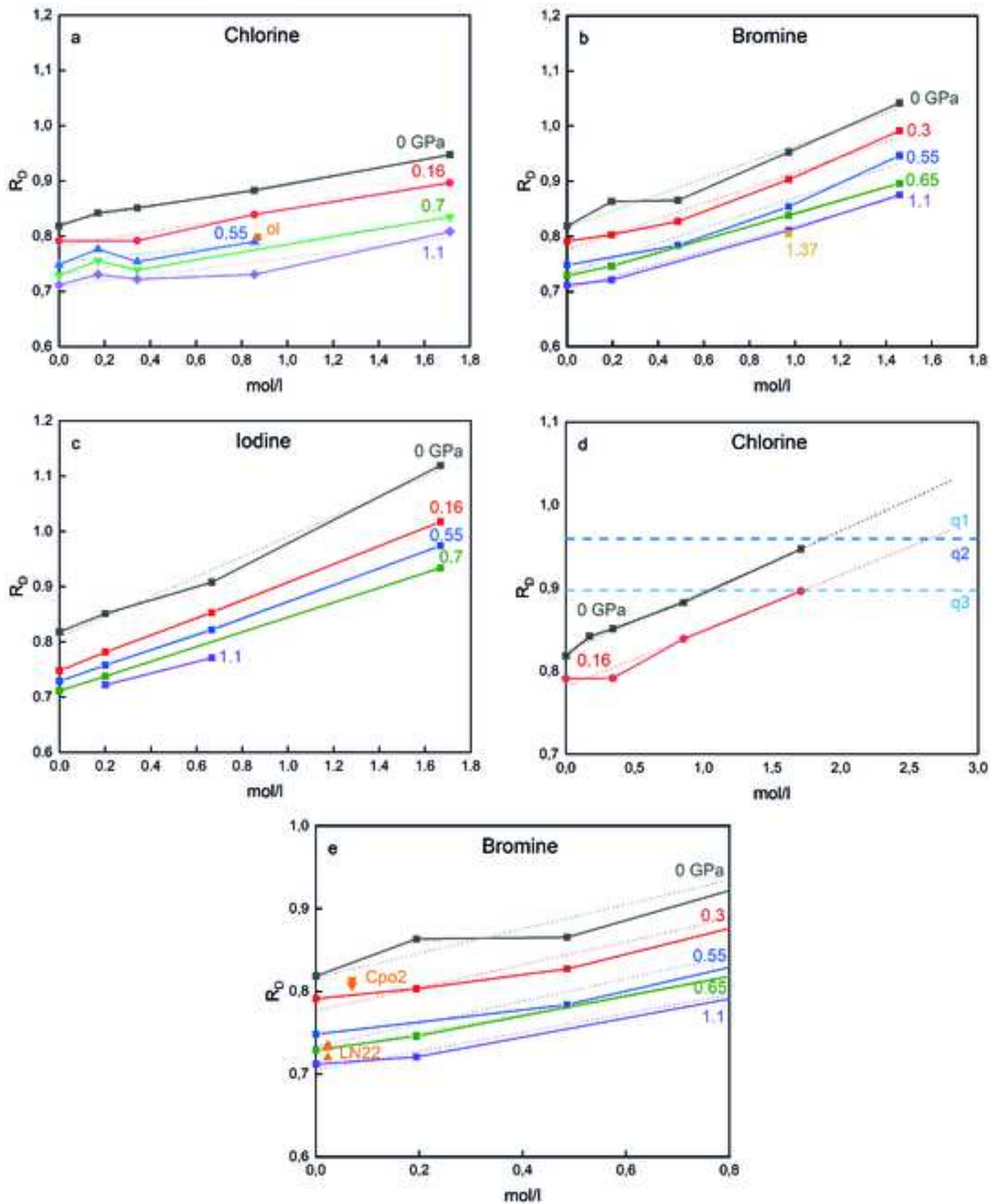
Figure 1

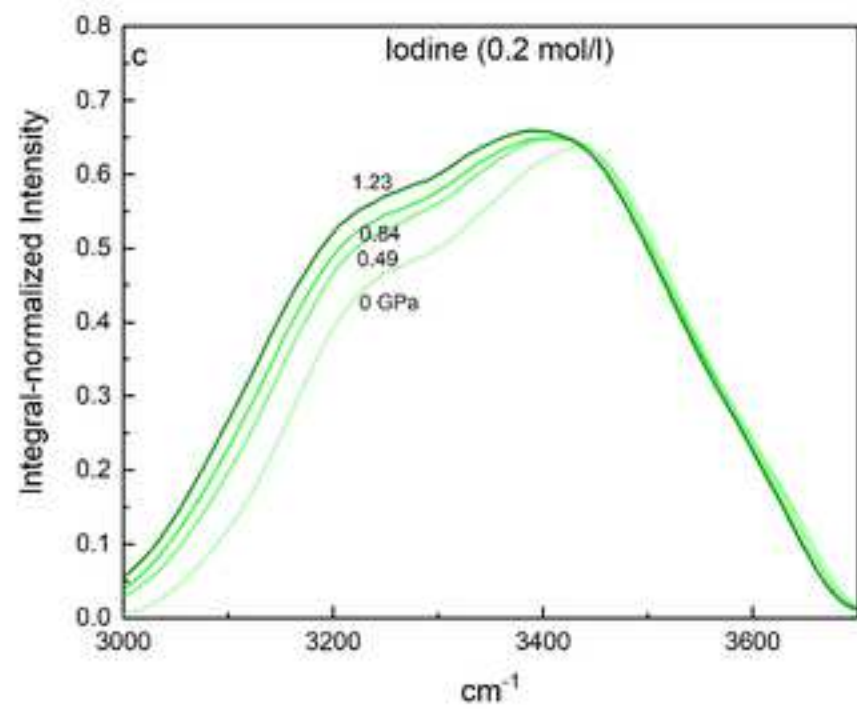
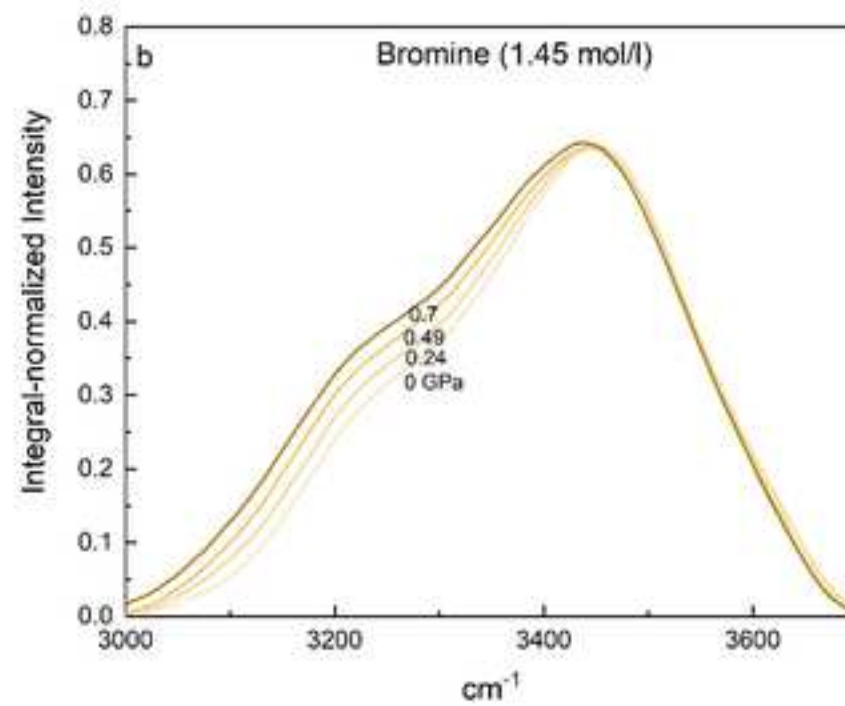
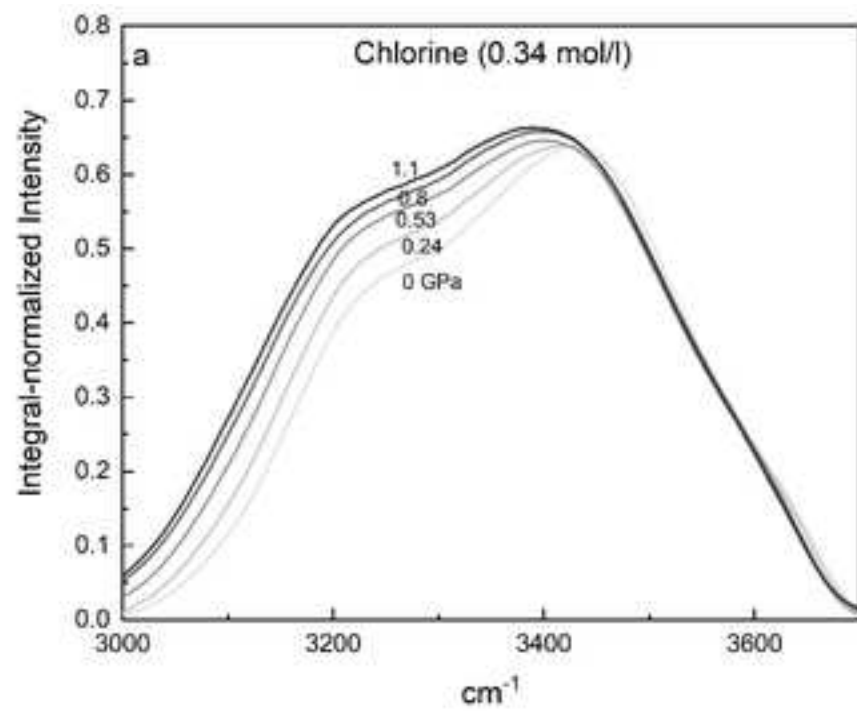


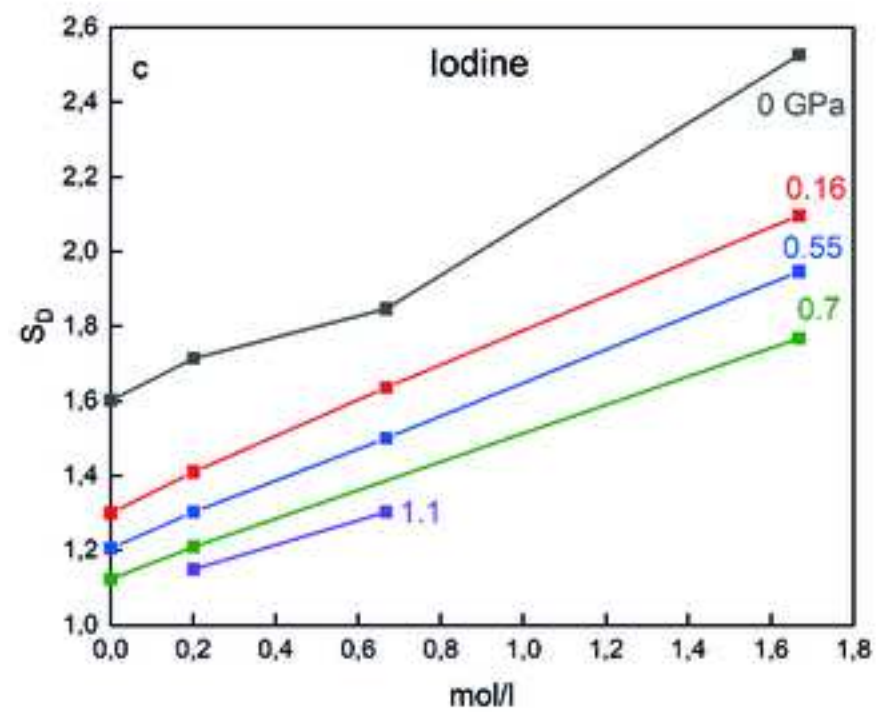
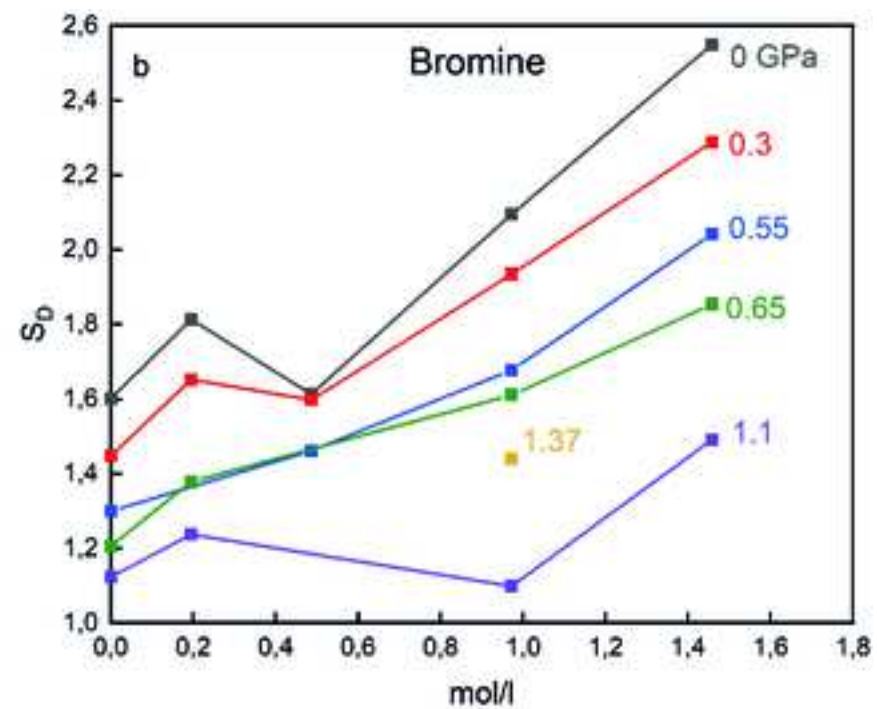
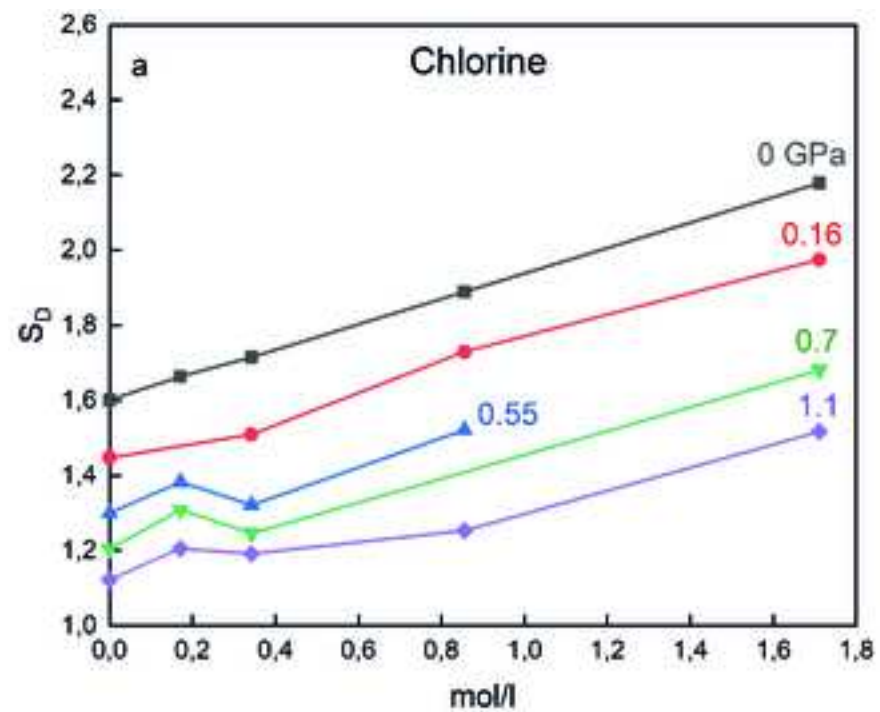












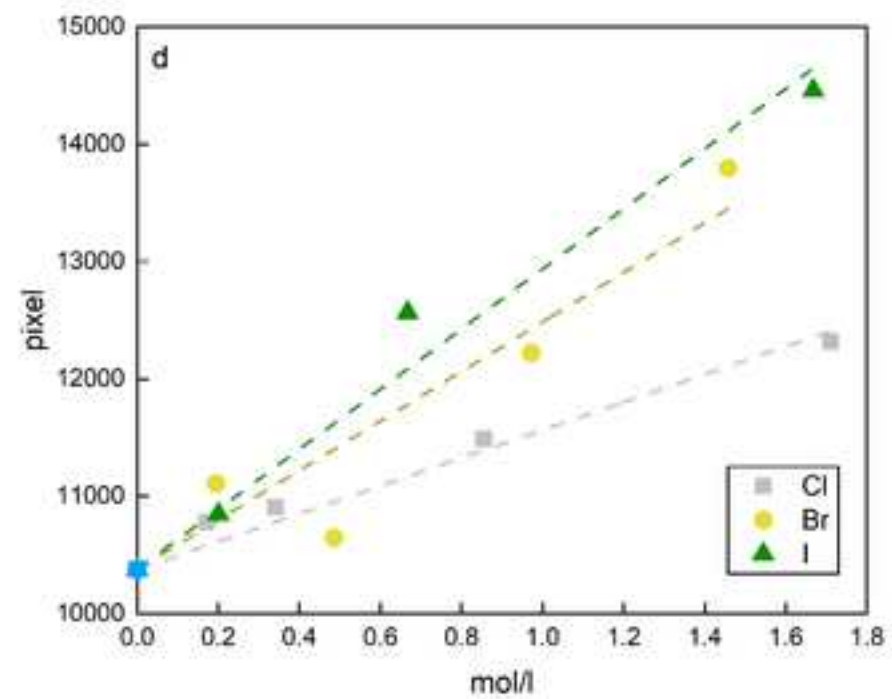
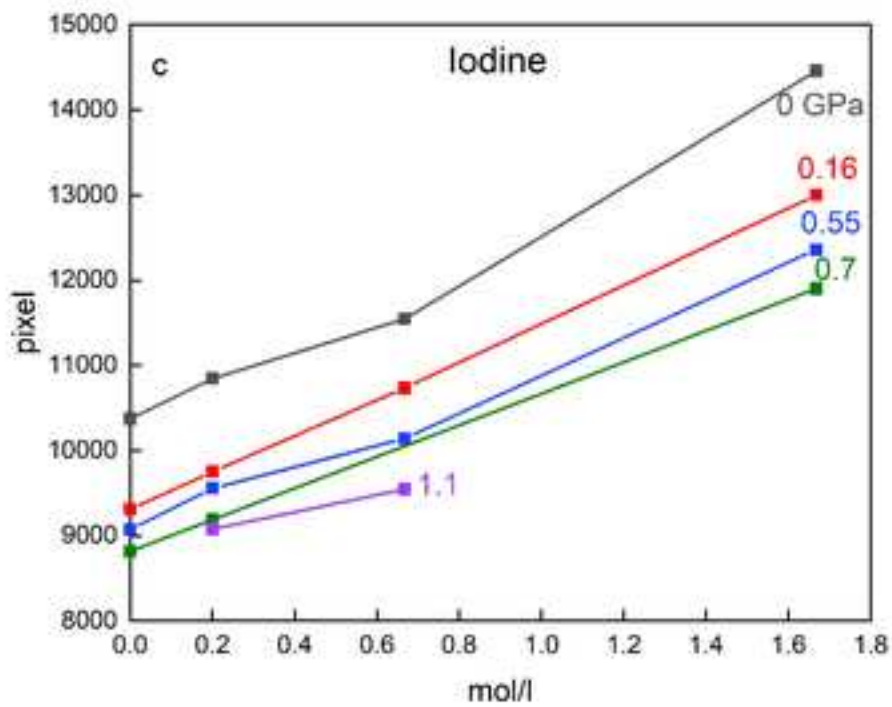
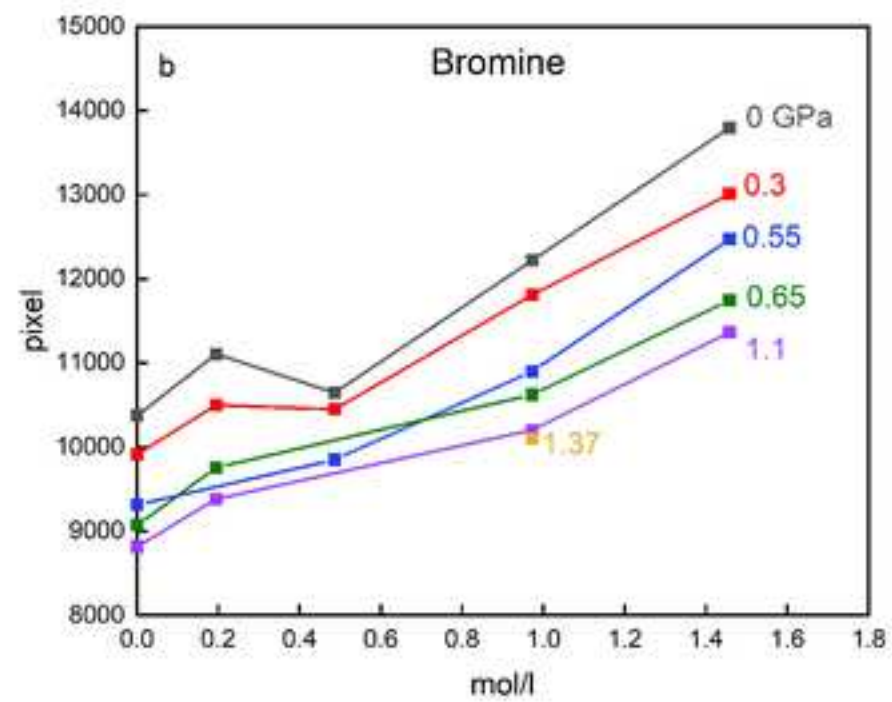
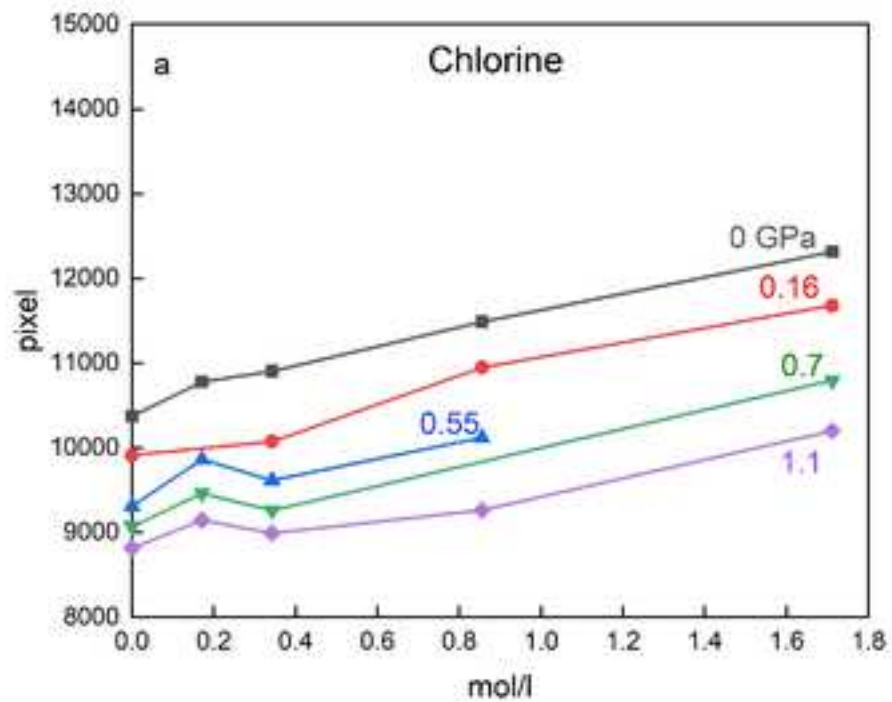


Table 1: Salt concentration in the starting solutions and maximum solubility values.

	NaCl				max(NaCl) ^a
g/l	10	20	50	100	317
mol/l	0.17	0.34	0.86	1.71	5.42
wt.%	0.99	1.96	4.76	9.09	24.07

	NaBr				max(NaBr) ^a
g/l	20	50	100	150	905
mol/l	0.19	0.49	0.97	1.46	8.80
wt.%	1.96	4.76	9.09	13.04	47.51

	NaI			max(NaI) ^a
g/l	30	100	250	1793
mol/l	0.20	0.67	1.67	11.96
wt.%	2.91	9.09	20.00	64.20

^a maximum solubility in H₂O at 20 °C and ambient pressure.

Declaration of interests

The authors declare that they have no known competing financial interests or personal relationships that could have appeared to influence the work reported in this paper.

The authors declare the following financial interests/personal relationships which may be considered as potential competing interests:

Tobias Grutzner reports financial support was provided by European Commission. Helene Bureau reports financial support was provided by French National Research Agency. If there are other authors, they declare that they have no known competing financial interests or personal relationships that could have appeared to influence the work reported in this paper.



Click here to download Research Data
<https://data.mendeley.com/datasets/tnckfpjcv/1>

